Mikal Solstad Øiaas

Exploring the cardioprotective effects of miR-210 in doxorubicin-treated cardiomyocytes

Masteroppgave i farmasi
Veileder: Morten Andre Høydal
Medveileder: Nathan Scrimgeour and Gurdeep Marwarha
Mai 2024

NTNU
Kunnskap for en bedre verden

Mikal Solstad Øiaas

Exploring the cardioprotective effects of miR-210 in doxorubicin-treated cardiomyocytes

Masteroppgave i farmasi
Veileder: Morten Andre Høydal
Medveileder: Nathan Scrimgeour and Gurdeep Marwarha
Mai 2024

Norges teknisk-naturvitenskapelige universitet
Fakultet for medisin og helsevitenskap
Institutt for klinisk og molekylær medisin

NTNU
Kunnskap for en bedre verden

Abstract

Background: Doxorubicin (DOX) is a widely used chemotherapeutic drug in the treatment of cancer. Due to its cardiotoxic properties, the cumulative dose needs to be strictly controlled. Recent work suggests that microRNA-210 (miR-210) may have cardioprotective effects by inhibiting apoptosis. This study sought to examine the impact of miR-210 in mitigating DOX-induced cardiotoxicity in AC16 cardiomyocytes (CMs) and human induced pluripotent stem cell-derived CMs (hips-CMs).

Methods: AC16 CMs and hiPSC-CMs were treated with 5 µM DOX and 1 µM DOX, respectively. AC16 CMs were transfected with miR-210 overexpression or knockdown vector, or their respective control vectors. hiPSC-CMs were transfected with miR-210 mimic or a scramble sequence. Cell death was quantified by using the lactate dehydrogenase (LDH) assay. The multiwell microelectrode array (MEA) system was used to examine electrophysiological properties.

Results: When overexpressing miR-210, we observed a significant attenuation of DOX-induced cell death in both AC16 CMs and hiPSC-CMs. DOX and miR-210 was observed to alter electrophysiological properties of hiPSC-CMs, including field potential duration, beat period and depolarization characteristics.

Conclusion: In this study, miR-210 was shown to protect against DOX-induced cell death in AC16 CMs and hiPSC-CMs. While protecting against cell death, miR-210 altered electrophysiological properties of hiPSC-CMs. To better understand the therapeutic potential of miR-210 in mitigating DOX-induced cardiotoxicity, further research is required to explore the effects of miR-210 on electrophysiological properties in DOX-treated hiPSC-CMs.

Sammendrag

Bakgrunn: Doxorubicin (DOX) er et mye brukt kreftlegemiddel. På grunn av betydelig kardiotoksisitet må den kumulative dosen kontrolleres nøye. Studier har vist at mikroRNA-210 (miR-210) kan ha en beskyttende effekt på hjertemuskelceller ved å hemme apoptose. I denne studien ønsket vi derfor å undersøke den beskyttende effekten av miR-210 med hensyn til kardiotoksisitet indusert av DOX i hjertemuskelceller av typen AC16 og humane stamcelle-deriverte hjertemuskelceller (HSDH).

Metoder: Vi behandlet AC16 og HSDH-cellene med henholdsvis 5 µM og 1 µM DOX. AC16-cellene ble transfektert med en overutrykkende miR-210-vektor eller en inhiberende miR-210-vektor, eller med deres respektive kontrollvektorer. HSDH-cellene ble transfektert med miR-210 eller en kontrollsekvens. Celledød ble kvantifisert gjennom å måle mengden laktatdehydrogenase. Multiwell microelectrode array (MEA)-systemet ble brukt for å undersøke de elektrofysiologiske egenskapene hos HSDH-celler.

Resultater: Overuttrykk av miR-210 reduserte DOX-indusert celledød i AC16-cellene og HSDH-cellene. Både DOX og miR-210 endret de elektrofysiologiske parameterne målt ved hjelp av MEA-systemet.

Konklusjon: miR-210 viste seg å beskytte mot celledød indusert av DOX-behandling i både AC16- og HSDH-cellene. Samtidig som miR-210 hadde en beskyttende effekt mot celledød, så vi også påvirkninger på elektrofysiologiske egenskaper i HSDH-cellene. For å kartlegge den potensielle hjertemuskelcellebeskyttende effekten av miR-210, trengs mer forskning for å undersøke de elektrofysiologiske effektene av miR-210 i DOX-behandlede hjertemuskelceller.

Acknowledgements

Table of contents

Figures

Tables

Abbreviations

AM: Assay medium.

AMI: Acute myocardial infarction.

AP: Alkaline phosphatase.

APD: Action potential duration.

BAK: Bcl-2-homologous antagonist killer.

BAX: Bcl-2-associated X protein.

CVD: Cardiovascular disease.

DDR: DNA damage response.

DOX: Doxorubicin.

EV: Empty vector.

FBS: Fetal bovine serum.

ISCU: inhibiting iron-sulfur clusters.

KD: Knockdown.

LEAP: Local extracellular action potential.

MEA: Multiwell microelectrode array.

MI: Myocardial infarction.

MM: Maintenance Medium.

MRE: miRNA response elements.

OE: Overexpression.

PM: Plating Medium.

PNPP: Para-nitrophenylphosphate.

PUMA: p53 upregulated modulator of apoptosis.

ROS: Reactive oxygen species.

SERCA: SR Ca2+ ATPase.

1 Introduction

1.1 Cardiovascular disease

The prevalence and mortality of cardiovascular disease (CVD) are increasing globally. Additionally, the disease burden of CVD, expressed as disability-adjusted life years, is also increasing (1). CVD is the leading cause of death in the world today (2). The term CVD encompasses many different diseases: Coronary artery disease, which includes angina pectoris, myocardial infarction (MI) and heart failure, cerebrovascular disease, peripheral artery disease and aortic atherosclerosis (3).

There are a multitude of risk factors associated with CVD, such as an unhealthy diet, a lack of physical activity, dyslipidemia, diabetes, hypertension, and smoking, to name a few (4). In addition to these risk factors, several medical drugs can also have deleterious effects on the heart and therefore lead to CVD. Examples of such drugs include non-steroidal anti-inflammatory drugs, antihypertensives, tricyclic antidepressant drugs, and certain chemotherapeutics, such as the anthracyclines (5). Among the anthracyclines, doxorubicin (DOX) is particularly widely used, for example in cancers of the breasts, lungs, ovaries and the uterus, as well as different leukemias and lymphomas (6).

1.2 General aspects of chemotherapeutics and cardiotoxicity

The term chemotherapeutics encompasses several drug classes used mainly in the treatment of cancer. In this group, we find alkylating agents, antimetabolites, antimicrotubular agents, antibiotics, among others. The anthracyclines are classified as antimicrotubular agents, specifically as topoisomerase II inhibitors (7). Among the anthracyclines, we find the compounds daunorubicin, DOX, epirubicin, idarubicin and mitoxantrone (6).

Chemotherapeutics have a range of different side effects, some of which are general chemotherapeutic side effects, and some of which are specific for the drug in question. The more common side effects for chemotherapeutics as a group, are disturbances of the gastrointestinal tract, mucositis, fatigue, hair loss and pain (8). Some of the chemotherapeutics can also negatively affect the heart, but the manner in which they do so, and the severity of the affection, differ (6).

Chemotherapeutics-induced cardiotoxicity is divided into type 1 and type 2. Type 1 cardiotoxicity is broadly characterized by the irreversible death of cardiomyocytes, either by necrosis or apoptosis, while type 2 cardiotoxicity is broadly characterized by reversible cardiomyocyte dysfunction (9). Examples of anti-cancer drugs causing type 1 cardiotoxicity are the anthracyclines, the alkylating agents and the taxanes. Examples of anti-cancer drugs causing type 2 cardiotoxicity are proteasome inhibitors, tyrosine kinase inhibitors, HER2 targeting antibodies and HER2 targeting tyrosine kinase inhibitors (5).

Among the chemotherapeutics that can cause type 1 cardiotoxicity, the anthracyclines are particularly notorious (6). Given the frequent use of anthracyclines in general, and DOX in particular, coupled with the cardiotoxic risk that is associated with their use, a substantial clinical challenge has emerged, and it is a challenge that so far remains unsolved (9).

1.3 DOX and cardiotoxicity

1.3.1 Defining cardiotoxicity
Patients treated with DOX can develop cardiotoxic manifestations early or late, with early being defined as within one year of completing treatment with DOX, and late being defined as after one year after completion (9). Already within one week after treatment, an acute injury to the cardiac cells can take place. Myocarditis and pericarditis can occur, as well as electrophysiological disturbances such as changes to the ST- and T-waves, QT-interval prolongation and arrythmias (10). The incidence of these acute changes has been reported to be 11% (11). Although it was noted earlier that DOX causes type 1 cardiotoxicity, which is generally thought to be irreversible, DOX can also cause acute cardiotoxic manifestations that can be reversible, such as myocardial edema (12).

Chronic changes to the myocardium can also occur after DOX treatment, symptomatically similar to what is seen in dilated cardiomyopathy. Pathological changes to the cardiac tissue occur, with fibroblast proliferation, vacuolated myocytes, interstitial fibrosis and loss of myofibril function. The pathological changes culminate in both a systolic and diastolic dysfunction, which could give rise to heart failure (12). These changes become apparent after as little as 30 days, or even as much as after 10 years after treatment. The overall incidence of chronic DOX-induced cardiotoxicity is approximately 1.7%. However, if the cumulative dose is above 600 mg/m^2, the risk of developing cardiomyopathy can be as high as 36% (11, 12). If the patient develops congestive heart failure, 1-year mortality is as high as 50% (12).

Not all patients treated with DOX have an equal risk of being affected by its cardiotoxic properties. Several risk factors have been identified, such as female sex, hypertension, earlier exposure to radiation in the mediastinal area, concurrent treatment with cyclophosphamide, paclitaxel or trastuzumab, younger and older age, and a high cumulative dose of anthracyclines given. The cumulative dose given appears to be the strongest risk factor (6, 9, 12, 13).

1.3.2 Mechanism behind DOX-induced cardiotoxicity
As noted earlier, DOX is categorized as an anthracycline generally and a topoisomerase IIb inhibitor (TOP2B) specifically (14). While the mechanism behind its anticancer effects is still under investigation, it has been established that DOX affects the DNA through intercalation, topoisomerase II inhibition and production of reactive oxygen species (ROS), as well as affecting mitochondrial function and triggering various pathways of cell death, such as apoptosis, ferroptosis, necrosis, pyroptosis and autophagy (14). The mechanisms that seem to dominate in DOX-induced cardiomyopathy are oxidative stress, the formation of free radicals and apoptosis (15, 16).

DOX causes ROS formation in several ways. DOX reacts with components in the cell, such as NADH dehydrogenase, and undergoes redox cycling. During redox cycling, DOX is reduced to a semiquinone free radical. The semiquinone free radical can react with molecular oxygen, forming superoxide anions. Exposing cells to DOX also leads to mitochondrial dysfunction. DOX accumulates in the inner mitochondrial membrane, interacting with cardiolipin, disrupting the function of mitochondria. When the electron transport chain of the mitochondria is affected, superoxide radicals can be formed. In addition, DOX can form a complex with iron, which in turn can cause the formation of reactive hydroxyl radicals (15). On top of causing ROS formation, DOX itself leads to a

decrease in antioxidants found in the cell, such as superoxide dismutase and glutathione peroxidase, lowering the cell's natural defense against ROS. Due to the significant increase in ROS and decrease in antioxidants, DOX treatment therefore subjects the cells to significant oxidative stress, which can lead to apoptosis and other forms of cell death (17).

1.3.2.1 DOX-induced cell death

As previously mentioned, exposure to DOX can cause cell death through various mechanisms. As a consequence of their significance in DOX-induced cell death, autophagy, pyroptosis and ferroptosis will be briefly mentioned, while the focus will be on apoptosis. In autophagy, depletion of vital cellular components can occur when autophagosome formation is increased due to DOX exposure, leading to cell death. An inflammatory mechanism of cell death, pyroptosis, can also occur. Through activation of inflammasomes due to ROS generation and direct activation by DOX, the cell undergoes lysis after pores have formed in the plasma membrane. In ferroptosis, lipid peroxidation is the result of both an inhibition of glutathione peroxidase 4, as well as an increase in intracellular free iron, which can contribute to an increase in lipid peroxidation. Consequently, lipids in the plasma membrane get damaged, and cell death occurs (14).

The increase in oxidative stress due to inhibition of endogenous antioxidants combined with an increase in ROS formation, can lead to damage of both nuclear DNA and mitochondrial DNA, as well as lipids and proteins in the cell. Consequently, due to the oxidative stress experienced by the cell, apoptosis can be triggered through various mechanisms. One such mechanism is cytochrome C release from the mitochondria to the cytoplasm. Through disruption of the mitochondrial membrane due to ROS, cytochrome C leaks into the cytoplasm, which can trigger apoptosis through caspase activation (15). Upon reaching the cytoplasm, cytochrome C forms a complex, the apoptosome, through binding with the protein apoptotic protease activating factor-1 (APAF1). The apoptosome then activates procaspase-9 into caspase-9, which in turn causes activation of caspase-3 and caspase-7, forcing the cell to undergo apoptosis. (18).

Another mechanism through which apoptosis is triggered, is by a DNA damage response (DDR). The damage to the DNA from ROS formation triggers an activation of p53, a protein capable of inducing apoptosis if sufficient damage has been inflicted upon the cell (15, 19). There are several ways in which p53 can induce apoptosis. Upon damage to the DNA, p53 is stabilized and p53 levels increase. Consequently, p53 induces the expression of several genes involved in apoptosis, including p53 upregulated modulator of apoptosis (PUMA), Bcl-2-homologous antagonist killer (BAK) and Bcl-2-associated X protein (BAX) in the Bcl-2-family. BAX and BAK are involved in pore formation in the mitochondrial membrane, exacerbating the release of cytochrome C, contributing to apoptosis as previously described. PUMA inhibits proteins with anti-apoptotic functions, potentiating the effects of BAX. In addition to inducing apoptosis through acting as a transcription factor, P53 also has the ability to bind directly with the mitochondrial membrane, further increasing the release of cytochrome C, which can then bind to APAF1, as described above (20).

In addition to inducing cell death, DOX also affects electrophysiological properties of cardiomyocytes, increasing the risk of developing abnormal cardiac function (21).

1.3.2.2 Electrophysiological effects of DOX

The cardiac action potential is divided up into five phases. During the first phase (phase 0), rapid depolarization occurs because of an opening of the Nav1.5 voltage-gated sodium channels, causing sodium influx. In phase 1, voltage-gated potassium channels (Ito) open, and potassium leaves the cell, with the result being a slight repolarization. During phase 2, there is a plateau in the action potential due to an influx of calcium through the Cav1.2 L-type calcium channel, as well as an efflux of potassium. Moving on to phase 3, a rapid repolarization occurs due to efflux of potassium through rapidly activating (Ikr) and slowly activating (Iks) potassium channels. In phase 4, the membrane potential has reached its resting state (22).

DOX has several effects on electrophysiological parameters in CMs. Due to the increase in oxidative stress, DOX inhibits the Nav1.5 voltage-gated sodium channel, decreasing the speed by which sodium travels into the cell, thereby reducing depolarization spike velocity (21). One plausible mechanism is through an increase in ROS generation. ROS has been shown to induce retention of forkhead box protein O1 in the nucleus, thus suppressing transcription of the SCN5a gene coding for the Nav1.5 voltage-gated sodium channel (23).

In the plateau phase, DOX increases the amplitude of the calcium influx through L-type calcium channels, prolonging the depolarization phase and potentially increasing the action potential duration (APD) (21). With an increase in ROS due to DOX exposure, calcium levels in the cytosol can increase due to SR Ca2+ ATPase (SERCA) inhibition and increased ryanodine receptor (RyR) activity (24), thus plausibly increasing calcium influx during the plateau phase. Intracellular calcium levels and ROS generation are intertwined. ROS together with calcium can in turn cause an opening of the mitochondrial permeability transition pore, increasing ROS production, further worsening the oxidative stress, amplifying effects on calcium influx (25).

The repolarization phase has also been shown to be impacted after DOX administration. A decrease in potassium efflux due to inhibition of Ikr and Iks channels brings about a prolongation of the APD, which has been associated with the development of arrhythmias (21). Through intermediary steps, DOX induces activation of caspase-3 (15). Caspase-3 causes proteolysis of Kv7.1, a component of the Iks voltage-gated potassium channel, culminating in disruption of the potassium channel's structure. Consequently, the current through Iks is reduced, potentially contributing to QT-interval prolongation and arrythmias (26).

1.3.3 Prevention of DOX-induced cardiotoxicity

Preventing DOX-induced cardiotoxicity remains a significant challenge. While beta-blockers, ACE-inhibitors, angiotensin II receptor blockers and aldosterone antagonists are mainstays in the pharmacological treatment of heart failure (27), their use in preventing DOX-induced cardiotoxicity has not shown conclusively to be of benefit (28).

Dexrazoxane is the only drug that has been approved by the FDA and EMA for preventing DOX-induced cardiotoxicity. As previously mentioned, DOX can form a complex with iron, causing the formation of ROS. Dexrazoxane has traditionally been thought to work by binding to iron, thus preventing complex formation and subsequent ROS formation (29). More recently, dexrazoxane has been shown to also prevent binding between DOX and TOP2B, which protects the DNA from damage through preventing double-stranded breaks (30). The use of dexrazoxane is approved in children up to 16 years of age receiving a

dose over 300 mg/m^2 of DOX, as well as in women with advanced breast cancer who require a large cumulative dose of DOX (31). It has been reported that the use of dexrazoxane could increase the risk of secondary malignancy (32), but the risk appears to be small, if any (31). Because the mechanism behind the anticancer activity of DOX is in part due to inhibition of TOP2B, a possible reduction in anticancer activity when co-treating with dexrazoxane has been speculated, but not confirmed (31). A meta-analysis from 2019 examining the efficacy of dexrazoxane in preventing cardiotoxicity in breast cancer patients treated with anthracyclines and/or trastuzumab, found that while dexrazoxane decreased cardiac events, the quality of evidence was deemed too low to support wide implementation. The authors noted that addition of dexrazoxane did not affect the efficacy of the cancer treatment (33). Currently, limiting the cumulative dose of DOX appears to be the best way to prevent DOX-induced cardiotoxicity, along with adding dexrazoxane when indicated, and monitoring for cardiotoxicity through assessing ventricular function and B-type natriuretic peptide and troponin levels (34).

Recently, microRNAs (miRNAs), a form of non-coding RNA, have shown diagnostic and therapeutic potential in various diseases, including CVD (35). Among the non-coding RNAs, miRNAs have been extensively studied. Additionally, their presence and activity have been linked to drug resistance, cancer development and other conditions, making miRNAs interesting candidates to explore for diagnostic and therapeutic improvement (36, 37).

1.4 miRNAs

1.4.1 General function of miRNAs

miRNAs are a form of non-coding RNA involved in the regulation of gene expression. They can be classified according to both their length (the number of nucleotides) and function. miRNAs are approximately 22 nucleotides in length. The group of non-coding RNA encompasses many different RNA molecules, such as microRNAs, Piwi-interacting RNAs, small nucleolar RNAs, small interfering RNAs and small nuclear RNAs. The amount of non-coding RNA far exceeds the amount of coding RNA. In fact, it has been suggested that 99% of the mammalian cell's RNA is non-coding RNA, suggesting the importance of these RNA molecules (36).

In the biogenesis of miRNAs, transcripts made by RNA polymerase II/III are processed through either a canonical pathway or non-canonical pathways. Only the canonical pathway will be described here, as it is the dominant one. The transcript made by polymerase II/III can come from either a protein-coding region of the DNA or an intergenic region (non-protein coding) region of the DNA. In the canonical pathway, the transcript starts out as pri-miRNA. Processing of the pri-miRNA occurs through a microprocessor complex. This microprocessor complex has both an RNA-binding protein and a ribonuclease III enzyme, called DiGeorge Syndrome Critical Region 8 (DGCR8) and Drosha, respectively. After processing of the pri-miRNA through motif-recognition by DGCR8 and cleavage by Drosha occurs, a pre-miRNA molecule is formed, ready to be transported from the nucleus to the cytoplasm. Once the pre-miRNA has been transported to the cytoplasm through the action of an exportin 5/RanGPT complex, further processing occurs through the removal of a terminal loop by the RNase III endonuclease Dicer. A mature miRNA duplex has now been produced, but before it can act upon its targets, it must first be loaded onto an argonaute protein. Both the 5' and 3' ends can be loaded onto AGO, depending on what the desired product is for the cell in

question. After the mRNA has been loaded onto AGO, a complex is formed: The miRNA-induced silencing complex (miRISC). Both the canonical pathways and the non-canonical pathways lead to the formation of this complex, and it is first upon the formation of miRISC that miRNA can begin to exert its effects (38).

The mature mRNA has miRNA response elements (MRE), where typically the 5' end or the 3' end of the miRNA in miRISC can bind through complementary base pairing. Should this base pairing be fully complementary, slicing of the target mRNA occurs through the endonuclease action of AGO2, leading to the destruction of the mRNA, and the degradation of the miRNA because of dissociation between AGO and the miRNA. Should this base pairing only be partially complementary, which is normally the case in humans, the endonuclease activity of AGO remains inactive. AGO then recruits different proteins, for example the GW182 family, ultimately leading to mRNA poly(A)-deadenylation and decapping, ending with degradation of the mRNA through activity of an exoribonuclease (38). In addition to being able to interact with the 5' or the 3' end of the target mRNA, coding sequences can also have MRE. Translational inhibition is the outcome of such an interaction, but an increase in the rate of translation has also been shown to happen (39).

miRISC can also induce translational repression without degrading the actual target mRNA. In protein synthesis, the ElF4F translation initiation complex needs to be assembled in order to recruit the ribosome to the mRNA (39). miRISC appears to dissociate the EIF4F complex, thus inhibiting the initiation step of translation (40). In addition to affecting translation, transcription can also be affected by miRISC. In the nucleus, it appears that miRISC can interact with promoter regions, either activating or inhibiting transcription. The mechanisms behind how this happens are not entirely clear, but it has been postulated that the action of RNA polymerase II can be inhibited by the binding of miRNA to the promoter region on the target DNA, effectively hindering the polymerase in binding to the promoter region. It has also been shown that miRISC can bind to the TATA-box of non-polymerases, such as insulin and calcitonin, with the effect of increasing the level of transcription (40).

1.4.2 The role of miRNAs in cancer and CVD

miRNAs have been shown to play a role in many different diseases, such as cancer and CVD. In cancer, both upregulation and downregulation of different miRNAs has been observed. It has been shown that different miRNAs can function as tumor suppressor genes and oncogenes, such as let-7 and miR-155, respectively (41). Specific patterns for specific types of cancer have emerged. In ovarian cancer, an upregulation of miR-200a, miR-200c and miR-141, along with a downregulation of miR-199a, miR-140, miR-145 and miR-125bl has been shown (42). In CVD, miRNAs show promise both as biomarkers and as a treatment. An elevation in miR-208b and miR-499 has been observed after acute myocardial infarction (AMI) and viral myocarditis (43). Therapeutically, inhibition of miR-25 has been shown to reduce fibrosis in mice with heart failure (44), and treatment with a miR-92a inhibitor was observed to lead to a reduction in infarct size after ischemia and reperfusion in a porcine model (45).

In ischemic heart disease, ischemia-reperfusion (I-R) injury is regarded as an important contributor to cell death (46). miR-210 has emerged as an interesting regulator of apoptotic cell death in I-R injury. During the hypoxia stage, miR-210 inhibits the intrinsic apoptotic pathway, thus contributing to the survival of cardiomyocytes. In the

reperfusion stage, however, miR-210 exacerbates cell death through activation of the extrinsic apoptotic pathway (47).

1.4.3 miR-210 in cardiovascular disease

miR-210 has been described as a so-called master hypoxamir because of its upregulation in many different cell types under hypoxia. Under hypoxic conditions, the hypoxia-inducible factors HIF1α and HIF2α cause an increase in miR-210 gene expression through interaction with the hypoxia response element on the miR-210 promoter region (48).

miR-210 inhibits the translation of mRNA coding for caspase 8 associated protein 2 (CASP8AP2), a protein important in Fas-induced apoptosis, increasing the survival of stem cells exposed to hypoxic conditions (49). In AC16 cardiomyocytes (CMs) subjected to hypoxia, miR-210 was found to reduce the activity of GSK3β. The inhibition of GSK3β led to a reduction of cytochrome C release through inhibiting the insertion of BAX and BAK in the outer mitochondrial membrane. The reduction in cytochrome C release further lessened the activation of caspase-3, a vital caspase in apoptotic cell death, thus protecting the AC16 CMs against cell death (50). In the mitochondria, miR-210 has several targets important in the electron transport chain. By inhibiting NADH: Ubiquinone Oxidoreductase Subunit A4, Succinate Dehydrogenase Complex Subunit D and Cytochrome c Oxidase Assembly Factor 10, miR-210 facilitates a shift in the mitochondrial metabolism from oxidative phosphorylation to glycolysis, reducing the need for oxygen to produce ATP (51). In addition, miR-210 causes downregulation of glycerol-3-phosphate dehydrogenase, inhibiting ROS generation (52).

In vivo, a rodent model using transgenic mice overexpressing miR-210 exposed to MI and ischemia/reperfusion injury through permanent and temporary ligation of the left-anterior-descending coronary artery, respectively, has shown that overexpressing miR-210 leads to an increase in neovascularization around the infarction, an attenuation of apoptosis of the cardiac tissue, and attenuation of cardiac output decrease (53). Another study with a similar experimental setup, found a reduction in apoptosis, an increase in angiogenesis and infarct size reduction in mice overexpressing miR-210 (54).

As previously mentioned, DOX exposure induces cell death and electrophysiological disturbances primarily through affecting free radical formation, oxidative stress and apoptosis (15, 16). As shown above, miR-210 modulates apoptosis and free radical formation, affecting both cell death and electrophysiology in CMs (49, 50, 52-54). Given the intersection between mechanisms behind DOX-induced cardiotoxicity and the effects of miR-210, we decided to further explore the effects of miR-210 on cell death and electrophysiology in AC16 CMs and human induced pluripotent stem cell cardiomyocytes (hiPSC-CMs) treated with DOX.

2 Aims and hypothesis

The aims of this thesis were:

1: To elucidate the effect of DOX and miR-210 on cell death in AC16 CMs and hiPSC-CMs.

2: To characterize the electrophysiological effects of DOX and miR-210 in hiPSC-CMs.

The hypotheses were:

1: miR-210 protects AC16 CMs and hiPSC-CMs from DOX-induced cell death.

2: miR-210 alters the electrophysiological properties in DOX-treated hiPSC-CMs.

3 Materials and methods

3.1 AC16 CMs

AC16 CMs (Sigma-Aldrich, Darmstadt, Germany) were utilized in this study. These cells are human CMs derived from ventricular cardiac tissue (55). The AC16 cell line shows a low variability in its response to stimuli and is an appropriate model for studying responses to cardiac insult (56). We therefore elected to use this cell line for the investigation of the effects of DOX and miR-210 in CMs with regards to cell death. For a general overview of the experimental outline, see figure 1.

3.1.1 Thawing, plating and subculturing

A vial containing AC16 cells was removed from a liquid nitrogen tank and allowed to thaw in a 37°C water bath. The contents of the vial were gently mixed using a small pipette, then transferred into a 50 mL tube. For culturing, medium consisting of Dulbecco's modified eagle's medium nutrient mixture F12 (DMEM/F12) (Thermo Fisher Scientific, Waltham, MA, USA), 12.5% fetal bovine serum (FBS) (Sigma-Aldrich, Darmstadt, Germany) and 1% antibiotic/antimycotic solution (Sigma Aldrich, Darmstadt, Germany) were prepared. DMEM mixed with FBS and antibiotic/antimycotic solution is hereafter called prepared DMEM. Between 10 to 15 mL of prepared DMEM warmed to 37°C was added to the tube. The tube was then centrifuged at 500 x g for three minutes to pellet the cells. The supernatant was aspirated, and the cell pellet was first resuspended in 1 mL of prepared DMEM, after which an additional 8 mL of prepared DMEM was added. Lastly, 2 mL of the cell suspension mix was added to four 100 mm culture plates, and each culture plate received an additional 10 mL of prepared DMEM. The cells were maintained in an incubator at 5% CO2 and 37°C, with a tray of sterile water placed inside the incubator to ensure proper humidity. Incubation is hereafter understood to be at 37°C unless otherwise specified.

Once the cells had reached approximately 90% confluency, subculturing took place as needed to fulfill future experimental requirements. The general procedure was as follows. The media was aspirated from the culture plate. Trypsin solution (Cytiva, Marlborough, MA, USA) was incubated for approximately 20 minutes. Around 5 mL of trypsin solution was then added to the culture plate. Thereafter, the culture plate was placed back in the incubator for about 3 minutes. Trypsin activity was quenched with an equal volume of prepared DMEM. The cell suspension was visually inspected to see if sufficient trypsinization had taken place, and then transferred to a tube and centrifuged at 500 x g for three minutes. The supernatant was aspirated, and the cell pellet was resuspended in approximately 1 mL of prepared DMEM. The resuspended cells were further diluted to with additional prepared DMEM, before being distributed among as many new culture plates as needed. Lastly, the culture plates were placed in an incubator.

3.1.2 Transfection

The AC16 CMs were transfected with miR-210 overexpression (OE) vector (pEZX-MR04) (GeneCopoeia, Rockville, MD, USA, catalogue number HmiR0167-MR04) or its empty vector (EV) control (pEZX-MR04-scrambled) (GeneCopoeia, Rockville, MD, USA, catalogue number CmiR0001-MR04), or miR-210 knockdown (KD) vector (pEZX-AM01-

miR-210) (GeneCopoeia, Rockville, MD, USA, catalogue number HmiR-AN0317-AM01) or its EV control (pEZX-AM01-scrambled) (GeneCopoeia, Rockville, MD, USA, catalogue number CmiR-AN0001-AM01). A general transfection procedure will be described.

The transfection mixes were made with transfection vector, transfection reagent and DMEM without FBS and antibiotic/antimycotic solution. The transfection vector was either empty vector, miR-210 OE vector or miR-210 KD vector. The transfection reagent was Polyfect transfection reagent (Qiagen, Hilden, Germany). The ratio of transfection vector: transfection reagent: DMEM was 1:5:50. In preparing the transfection mix, the order of addition was transfection vector mixed with Polyfect, then after five minutes DMEM was added. The respective transfection mixes were incubated for 30 minutes before being added to the cell suspension during the subculturing process. The AC16 CMs were then ready to be treated with either DOX (Sigma-Aldrich, Darmstadt, Germany) or sterile water (vehicle) (B. Braun, Meisungen, Germany). A total of 16 culture plates with confluent AC16 CMs were aspirated and treated with 5 mL trypsin. The trypsin was quenched after around three minutes with 5 mL prepared DMEM. The cell suspensions were then collected in four 50 mL tubes. Subsequently, the cell suspensions were centrifuged at 500 x g for 3 minutes. The supernatant was aspirated, and the pellets were resuspended in 1 mL media. After this, 500 µL of the resultant cell suspensions was put into two new 15 mL tubes, each tube containing a number of cells equivalent to two confluent culture plates. A total of eight tubes with 500 µL cell suspension were now ready to receive the transfection mix. A total of 336 µL of the appropriate transfection mix was added to each tube, yielding four tubes with EV and four tubes with miR-210 KD or OE. A total of 400 µL of the transfected cell suspension was added to each of the 16 culture plates, giving rise to eight plates with EV and eight plates with miR-210 KD or OE, ready for being treated with either 5 µM DOX or vehicle.

After transfection, the cells were left overnight in the incubator before being treated with DOX.

3.1.3 DOX treatment
After overnight incubation, we treated the AC16 CMs with DOX or vehicle. We chose a concentration of 5 µM DOX, as this has been shown in previous work to elicit substantial LDH release (57). Treatment duration was 24 hours. DOX was dissolved in vehicle, and thereafter diluted with prepared DMEM to give a terminal concentration of 5 µM. Vehicle was diluted in prepared DMEM. The respective solutions were incubated for 30 minutes. Eight plates were then treated with DOX, and eight plates were treated with vehicle, yielding four experimental groups with four plates each. Plates transfected with EV and treated with vehicle was defined as control. After treatment, the plates were put back into the incubator for 24 hours before harvesting took place.

3.1.4 Harvesting of media and protein fraction from AC16 CMs
A 100:1 mix of RIPA (radioimmunoprecipitation) lysis buffer (Santa Cruz Biotechnology, Dallas, TX, USA) and protease and phosphatase inhibitor (Santa Cruz Biotechnology, Dallas, TX, USA) were used to harvest the protein fraction. After 24 hours of DOX treatment, the media was aspirated from the plates and stored for later analysis at -20°C. An amount of 1 mL cold lysis buffer mix was added to the plates. The plates were scraped down with a cell scraper, and the resulting liquid was collected into 1.5 mL tubes and put on ice for 10 minutes. The tubes were then centrifuged at 4°C, 12 000 x g for 10 minutes. The supernatant was then collected and stored at -80°C pending future assays.

3.1.5 LDH assay

The LDH assay was used as a measure of cell death. During cell death, the cell membrane is compromised and LDH leaks into the media. The LDH amount is directly related to cell death (58).

A 96-well plate pre-coated with LDH capture antibody (Santa Cruz Biotechnology, Dallas, TX) USA was used. The LDH assay was done over a period of four days. The washing procedure between the different steps was as follows. First, the well contents were aspirated. Then, 200 µL of tris-buffered saline with 0.1% *v/v* Tween-20 (TBS-T) was added, followed by a five-minute incubation period on a shaker. The washing procedure was repeated a total of three times before proceeding to the next step.

On day one, wells were loaded with 50 µL media taken from the samples, together with an appropriate volume of PBS. The plate was incubated overnight on a shaker at 4°C.

On day two, wells were loaded with LDH-A and LDH-B detection antibody (Novus Biologicals/Bio-Techne, Abingdon, United Kingdom), either alone or together with blocking peptide as appropriate, and incubated overnight at 4°C on a shaker.

On day three, the wells were loaded with secondary antibody conjugated to alkaline phosphatase (AP) (Sigma-Aldrich, Darmstadt, Germany). After incubation for 2.5 hours on a shaker at room temperature, the wells were washed and para-nitrophenylphosphate (PNPP) was added. Lastly, the wells were left on a shaker at room temperature overnight. On day four, the plate was read.

The plates were read using Varioskan LUX Multimode Microplate Reader (Thermo Fisher Scientific, Waltham, MA, USA), with the software SkanIt Software 6.1 RE for Microplate Readers RE version 6.1.0.51 (Thermo Fisher Scientific, Waltham, MA, USA). The absorbance was measured at 405 nanometers.

3.1.6 miR-210 hybridization assay

The protein content of the lysate samples was adjusted to the same level through the Bradford assay, an assay used for determining the protein concentration (59). The miR-210 hybridization assay was done over a period of four days. A 96-well plate already coated with streptavidin and a biotin miR-210 capture probe (Qiagen Norge, Oslo, Norway) was used. Approximately 20 ug of protein is needed per well for this assay, and an appropriate sample volume was used to obtain the required protein level. The remaining volume in each well was filled with non-denaturing lysis buffer, reaching a total volume of 200 µL per well. There were four experimental groups, each group with four biological replicates. Each biological replicate had three technical replicates.

On day one, the samples were thawed on ice. Subsequently, 20 ug of protein was added to each well from the appropriate experimental group, and the remaining volume in each well was filled to reach 200 µL. The plate was incubated on a shaker at 4°C overnight.

On day two, the wells were washed as previously described. The wells were loaded with the digoxigenin-labeled detection probe (Qiagen Norge, Oslo, Norway), followed by a 2.5-hour incubation at room temperature on a shaker. For the next step, wells were loaded with digoxigenin antibody (R&D Systems, Minneapolis, MN, USA), either alone or together with blocking peptide as appropriate, and incubated overnight at 4°C on a shaker.

On day three, wells were loaded with secondary antibody conjugated to AP (Sigma-Aldrich, Darmstadt, Germany). After a 2.5-hour incubation at room temperature on a shaker, the wells were loaded with PNPP and incubated overnight on a shaker at 4°C. On day four, the plate was read in the same manner as previously described.
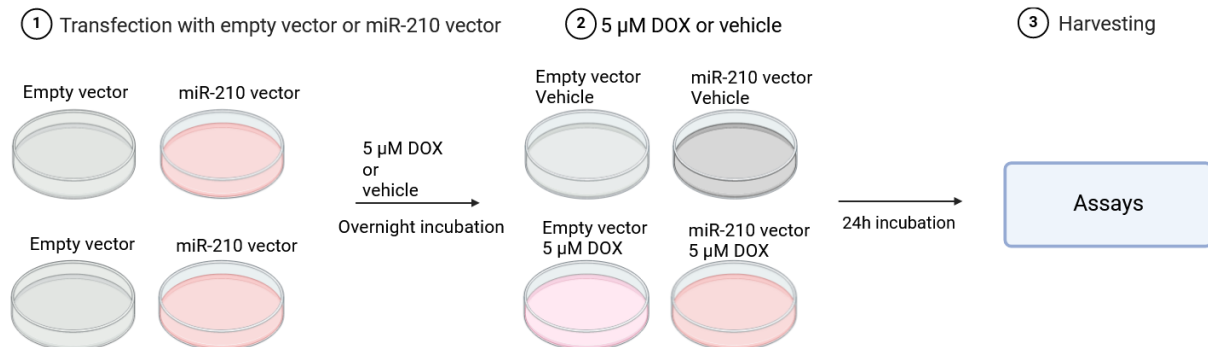
Figure 1: General procedure for transfection and DOX treatment in AC16 CMs. DOX: Doxorubicin, vehicle: Sterile water, miR-210: MicroRNA-210, OE: Overexpression, KD: Knockdown, CM: Cardiomyocyte. Created with BioRender.com.

The following table lists the antibodies and probes used in the LDH assay and miR-210 hybridization assay.

Table 1: List of antibodies and probes used in the LDH assay and the miR-210 hybridization assay.

Antibody Type	Source (catalogue number)	Host Species
LDH Capture Antibody	Santa Cruz Biotechnology, Dallas, TX, USA (sc-133123)	Mouse
LDH-A Detection Antibody	Novus Biologicals/Bio-Techne, Abingdon, UK (NBP1-48336)	Rabbit
LDH-B Detection Antibody	Novus Biologicals/Bio-Techne, Abingdon, UK (NBP2-38131)	Rabbit
Alkaline phosphatase-conjugated Secondary Antibody	Sigma-Aldrich, Darmstadt, Germany (A3687)	Goat
Biotin-labeled miR-210 Capture Probe	Qiagen Norge, Oslo, Norway (339,412 YCO0212944)	N/A
Digoxigenin-labeled miR-210 Detection Probe	Qiagen Norge, Oslo, Norway (339,412 YCO0212945)	N/A
Digoxigenin Antibody	R&D Systems, Minneapolis, MN, USA (MAB10386)	Rabbit

3.2 hiPSC-CMs and multiwell microelectrode array (MEA)

To further elucidate the effects of DOX and miR-210 on electrically active, excitable cells, we decided to use hiPSC-CMs (FujiFilm, Tokyo, Japan). HiPSC-CMs are widely used in pre-clinical testing of drugs to evaluate their cardiotoxicity. Due to their contractile ability, these beating CMs allow for assessing the functional effects of DOX and miR-210 (60).

For recording the electrical activity, we used the Maestro Pro multiwell microelectrode array (MEA) (Axion Biosystems, Atlanta, GA), with the software Axis Navigator version 3.11.1 (Axion Biosystems, Atlanta, GA) and Axis Metric Plotting Tool version 2.5.1 (Axion Biosystems, Atlanta, GA). The analysis was done with the following settings: The temperature was set at 37°C, with a CO_2 concentration of 5.0%. Before recordings were made, the cells were allowed a 10-minute equilibration period in the MEA system. For the statistical analysis, we decided to exclude wells with <10 active electrodes, measured before transfection had taken place.

3.2.1 Coating of MEA plate and thawing and plating of hiPSC-CMs

The coating, thawing and plating was done following the manufacturer's instructions. A fibronectin stock solution diluted to 50 ug/mL with D-PBS was made. The wells were then coated with 5 µL of the fibronectin solution. The MEA plate was then left in the incubator for one hour. A vial of hiPSC-CMs was thawed in a 37°C water bath for two minutes. The contents of the vial were transferred to a tube and rinsed with 650 µL FujiFilm iCell Plating Medium (PM) (FujiFilm, Tokyo, Japan). The PM with hiPSC-CMs were added drop-wise to the tube over 90 seconds, followed by addition of 1 mL of PM. The cell suspension was gently mixed and transferred to another tube.

Cell density was then determined by using the cell counter Countess II Automated Cell Counter (Thermo Fisher Scientific, Waltham, MA, USA). The cell suspension was centrifuged at 180 x g for five minutes. Afterwards, the supernatant was aspirated, and an appropriate volume of PM was added to achieve the desired density, a concentration of 10,000,000 cells/mL.

When plating the hiPSC-CMs, the fibronectin solution was aspirated, and each well received 5 µL of cell suspension, containing a total of 50,000 cells. The MEA plate was then put into the incubator for one hour to allow proper cell attachment. After one hour had passed, FujiFilm iCell Maintenance Medium (MM) (FujiFilm, Tokyo, Japan) was added to the plate. A total of 300 µL of MM was used per well, added in rounds of 150 µL in a slow manner to avoid washing away the attached cells. After addition of MM, the plate was put in the incubator. After the plating, MM was changed after 24 hours, thereafter every 48 hours until further experimental procedures were done.

3.2.2 Pilot experiment

We decided to run a pilot experiment on non-transfected cells to ascertain the appropriate DOX concentration. Before treatment of the cells with DOX, a media change was made to the iCell CardioTox Assay Medium (AM) (FujiFilm, Tokyo, Japan), as per the manufacturer's instructions. The wells were aspirated and rinsed with AM, before 270 µL AM was administered to all wells. The hiPSC-CMs were put back into the incubator for a four-hour equilibration period, after which DOX was applied. The following DOX treatment procedure was followed. A stock solution of DOX was made as previously described in section 3.1.3. The appropriate wells received 50 µM, 5 µM, 2 µM and 0.5 µM

DOX. For the control group, a mix of 1:1 of vehicle and AM was used. Based on the data gathered from the MEA system, we decided that additional wells were to be treated with 1 µM DOX the next day.

3.2.3 Transfection, DOX treatment, washout and harvesting

The cells were transfected six days after plating. The hiPSC-CMs were transfected with miR-210-3p mimic (Dharmacon, Lafayette, Colorado, USA) or a miR with no known complementarity to a human sequence (scramble) (Dharmacon, Lafayette, Colorado, USA). Treatment allocation was determined through randomization. The transfection procedure was as follows. Two transfection mixes were prepared with Lipofectamine RNAiMAX Invitrogen ((Thermo Fischer Scientific, Waltham, MA, USA), Opti-Mem 1x reduced serum medium ((Thermo Fischer Scientific, Waltham, MA, USA) and the appropriate miRNA. Lipofectamine and Opti-MEM were combined by diluting 2.4 µL Lipofectamine into 36.8 µL of Opti-MEM. In a separate tube, 4 µL of MiRNA was diluted into 36.8 µL of OptiMEM. Afterwards, the two solutions were mixed in a third tube. The transfection mixes were incubated at room temperature for 15 minutes before 20 µL of the appropriate mix was added to each well. Four hours after transfection, a complete medium change was performed to AM. The next day, the appropriate wells were treated with either 1 µM DOX or vehicle. The wells were randomized to the different treatment groups. On the day after, after the necessary recordings had been made, the media was harvested and stored at -20°C, and a media change was performed to assess the effects of a washout period, after which the cells were harvested. Harvesting was performed with Qiazol lysis reagent (Qiagen, Hilden, Germany). A total of 350 µL Qiazol was used per well, the contents were mixed by pipetting and then transferred to a 2 mL cryotube. Lastly, the cryotube was flash frozen in liquid nitrogen and stored at -80°C pending future assays.

For a summary of the experimental timeline, see figure 2.

Experimental Timeline
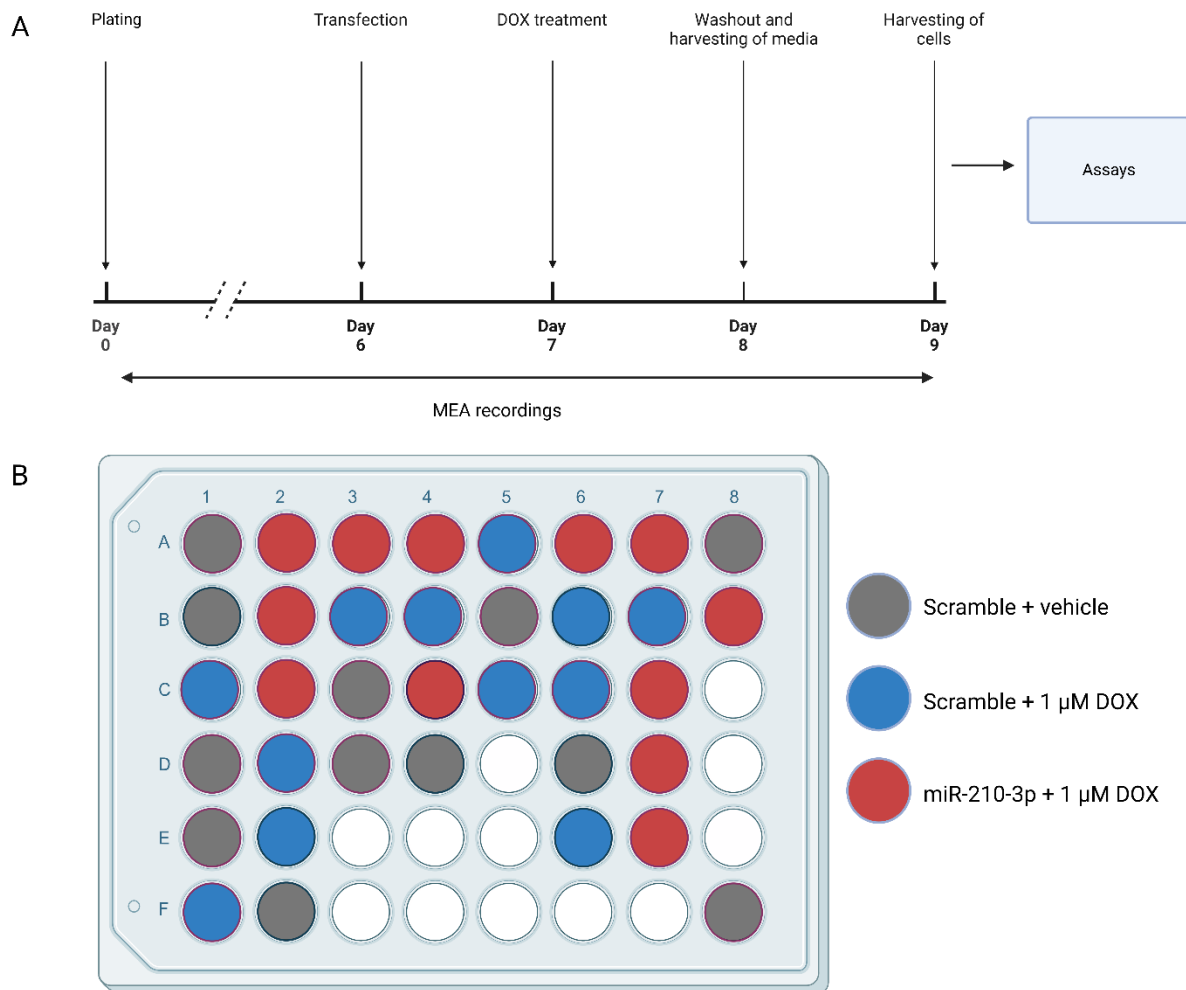
Figure 2: Experimental timeline (A) and MEA plate setup (B). MEA: Multiwell microelectrode array, DOX: Doxorubicin, vehicle: Sterile water, miR-210: MicroRNA-210. Created with BioRender.com.

3.2.4 LDH assay

An LDH assay was performed as described in section 3.1.5.

3.2.5 RNA extraction

To ascertain the levels of miR-210-3p, we performed a quantitative polymerase chain reaction (qPCR), involving RNA extraction, reverse transcription and qPCR.

The miRNeasy Mini Kit (Qiagen, Hilden, Germany) was used, containing the necessary collection tubes, miRNeasy spin columns and buffers. The RNA extraction was done as follows, following the manufacturer's instructions. Samples were allowed to thaw at room temperature for five minutes. A total of 70 µL chloroform was added to each sample-containing cryotube. The cryotubes were then vortexed at maximum speed for 15

seconds to ensure thorough mixing. The contents were transferred into Eppendorf tubes and centrifuged at 12,000 x g for 15 minutes at 4°C. After the centrifugation was complete, three distinct phases had formed, an upper aqueous RNA-containing phase, a middle white phase and a lower red organic phase.

The upper aqueous phase was transferred to a new collection tube. To the new collection tube, 100% ethanol (Antibac, Asker, Norway) was added at a volume of 1.5 times the volume of the transferred aqueous phase. The solution was mixed using the pipette, then pipetted into a RNeasy MinElute spin column. The spin column with its collection tube was subsequently centrifuged at 8,000 x g for 15 seconds. The flow-through was discarded. After this, 700 µL buffer RWT was added to the spin column, with another centrifugation taking place thereafter at 8,000 x g. The flow-through was again discarded. A wash of the column then took place with 500 µL buffer RPE, followed by centrifugation at 8,000 x g for 15 seconds, then discarding the flow-through. Subsequently, 500 µL buffer RPE was added again, and centrifugation at 8,000 x g took place for two minutes, and the collection tube was discarded. The RNA was then eluted by placing the column in a 1.5 mL collection tube and adding 50 µL RNase-free water (Qiagen, Hilden, Germany) was added to the membrane. The column was incubated with the RNase-free water for five minutes. Lastly, the collection tube was put in the centrifuge for one minute at full speed to gather the eluted RNA in the collection tube.

The amount of RNA was quantified through the use of NanoDrop 2000 spectrophotometer (Thermo Fischer Scientific, Waltham, MA, USA), with the Nanodrop 2000/2000c software version 1.6.198 (Thermo Fischer Scientific, Waltham, MA, USA). The results were used to quantify the amount of RNA to put into the reverse transcription.

3.2.6 Reverse transcription and qPCR

The miScript II RT kit (Qiagen, Hilden, Germany) was used, containing the necessary reagents. The protocol supplied by the company was followed. The RNA from the samples were thawed on ice. The buffers 10x Nucleics Mix and 5x miScript HiSpec Buffer were thawed at room temperature. The buffer miScript Reverse Transcriptase Mix was thawed on ice. The two first buffers were centrifuged briefly to collect the liquid at the bottom of the tube. A reverse-transcription master mix was prepared by mixing the 10x Nucleics Mix and the 5x miScript HiSpec buffer, using 20 µL and 40 µL, respectively. A total of 6 µL was added to each of nine Eppendorf tubes, after which an additional 12 µL was added from the appropriate sample RNA. Lastly, 2 µL of miScript Reverse Transcriptase Mix was added to each tube. The contents were mixed using the pipette and briefly centrifuged, and subsequently incubated at 37°C for one hour, followed by a five-minute incubation at 95°C. The samples with the complementary DNA (cDNA) were then diluted with 50 µL RNase-free water. Subsequently, the miScript PCR Starter Kit was used (Qiagen, Hilden, Germany), containing the necessary buffers and mixes. The protocol supplied by the company was then followed. A housekeeping gene (Rnu62) master mix was made, consisting of 437.5 µL 2x Sybr Green PCR Master Mix, 87.5 µL RNase-free water, 87.5 µL 10x miScript Universal Primer and 87.5 µL specific primer (Rnu62). A total of 20 µL of the housekeeping gene master mix was added to the appropriate wells. Thereafter, 2 µL of miScript Reverse Transcriptase Mix was added to each appropriate well. For the miR-210-3p, a miR-210-3p master mix was made, consisting of 437.5 µL 2x Sybr Green PCR Master Mix, 87.5 µL RNase-free water, 87.5 µL 10x miScript Universal Primer and 8.75 µL specific primer (miR-210-3p) (Thermo Fisher Scientific, Waltham, MA, USA). A total of 20 µL of the miR-210-3p master mix was added to the appropriate wells. Thereafter, 2 µL of miScript Reverse Transcriptase Mix was added to each

appropriate well. Lastly, 5 µL of sample was added to the correct wells. Upon completion, the PCR plate was taken to the CFX Opus 96 Real-Time PCR System (Bio-Rad, Hercules, California, United States), using the software Bio-Rad CFX Maestro 2.3 version 5.3.022.1030 (Bio-Rad, Hercules, California, United States) and the qPCR was finalized. The 2(-Delta Delta C(T)) method was used to assess the relative differences in gene expression between the experimental groups (61).

3.3 Statistical analysis

Graphpad Prism (version 10.2.1, GraphPad Software, San Diego, California USA, www.graphpad.com) was used for the data analysis. The Student's t-test, one-way ANOVA, two-way ANOVA, the uncorrected Fishers least significant difference test and Tukey's multiple comparison test were used to determine statistical significance. A p-value of < 0.05 was considered statistically significant.

4 Results

4.1 miR-210 attenuates cell death in DOX-treated AC16 CMs

To assess the effect of DOX and miR-210 on cell death in AC16 CMs, we performed an LDH assay. In EV-transfected cells, we found a significant increase in LDH release in cells treated with DOX compared to vehicle ($p < 0.0001$), indicating an increase in cell death in DOX-treated cells. In DOX-treated cells, we found significant attenuation of LDH release in cells transfected with miR-210 OE compared to EV ($p < 0.0001$) (figure 3A), indicating that miR-210 reduces cell death in DOX-treated AC16 CMs.

To determine the effect of DOX on miR-210 expression and to verify the efficacy of miR-210 overexpression, we performed a miR-210 hybridization assay. In EV-transfected cells, we found a significant increase in miR-210 levels in cells treated with DOX compared to vehicle ($p < 0.0001$). Comparing vehicle-treated cells, transfection with miR-210 OE caused a significant increase of miR-210 compared to control ($p < 0.0001$). In DOX-treated cells, we found a significant increase in miR-210 levels in cells transfected with miR-210 OE compared to EV ($p < 0.0001$) (figure 3B).

When knocking down miR-210 in DOX-treated cells, we found a significant increase in LDH release compared to cells transfected with EV ($p < 0.0001$) (figure 4A). This is in direct contrast to the finding in cells with miR-210 overexpression. To confirm the efficacy of the transfection procedure with miR-210 KD, another miR-210 hybridization assay was performed. We observed a significant decrease in miR-210 levels when transfecting with miR-210 KD in both vehicle-treated cells ($p < 0.01$) and DOX-treated cells ($p < 0.0001$) compared to transfecting with EV (figure 4B). The data from both experiments strongly suggest that miR-210 decreases cell death in DOX-treated AC16 CMs.

Figure 3: LDH release fold change (A) and miR-210 fold change (B) in AC16 CMs transfected with miR-210 OE vector or EV, treated with either DOX or vehicle for 24 hours. The data is presented as the mean ± SEM. SEM: Standard error of the mean, vehicle: Sterile water, EV: Empty vector, DOX: Doxorubicin, OE: Overexpression, miR-210: MicroRNA-210, LDH: Lactate dehydrogenase, CM: Cardiomyocyte. n=4 in all groups. Statistics were performed with a two-way ANOVA, with the uncorrected Fishers least significant difference test. **** = p < 0.0001.
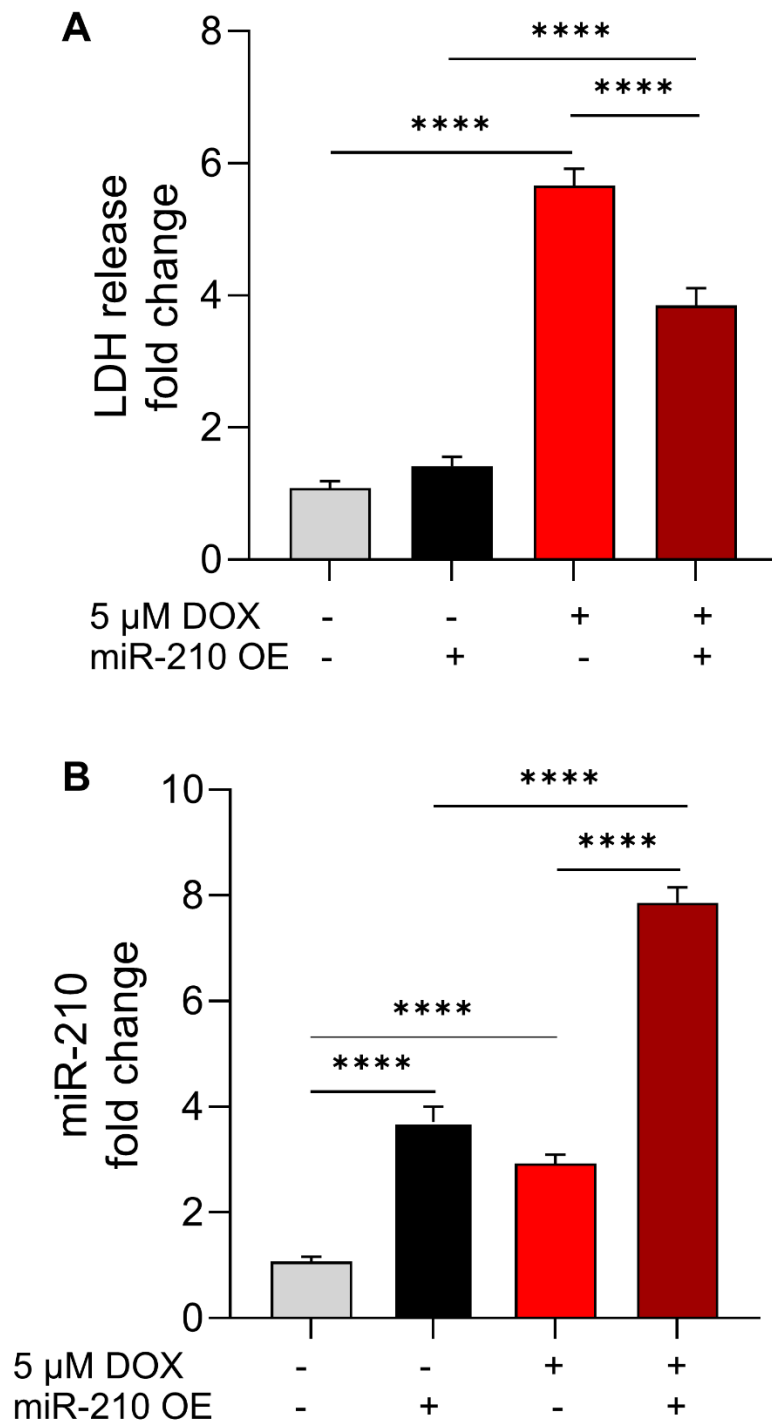
Figure 4: LDH release fold change (A) and miR-210 fold change (B) in AC16 CMs transfected with miR-210 KD vector or EV, treated with either DOX or vehicle for 24 hours. The data is presented as the mean ± SEM. SEM: Standard error of the mean, vehicle: Sterile water, EV: Empty vector, DOX: Doxorubicin, KD: Knockdown, miR-210: MicroRNA-210, LDH: Lactate dehydrogenase, CM: Cardiomyocyte. n=4 in all groups. Statistics were performed with a two-way ANOVA, with the uncorrected Fishers least significant difference test. ** = p < 0.01, **** = p < 0.0001.
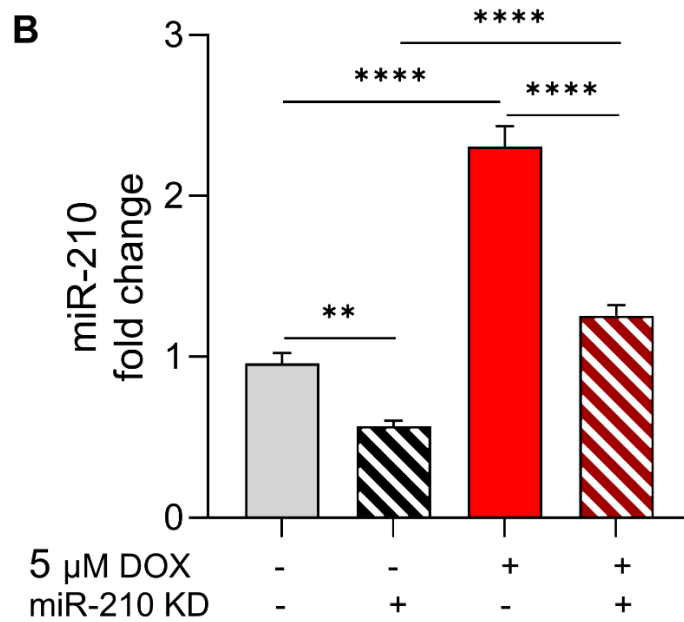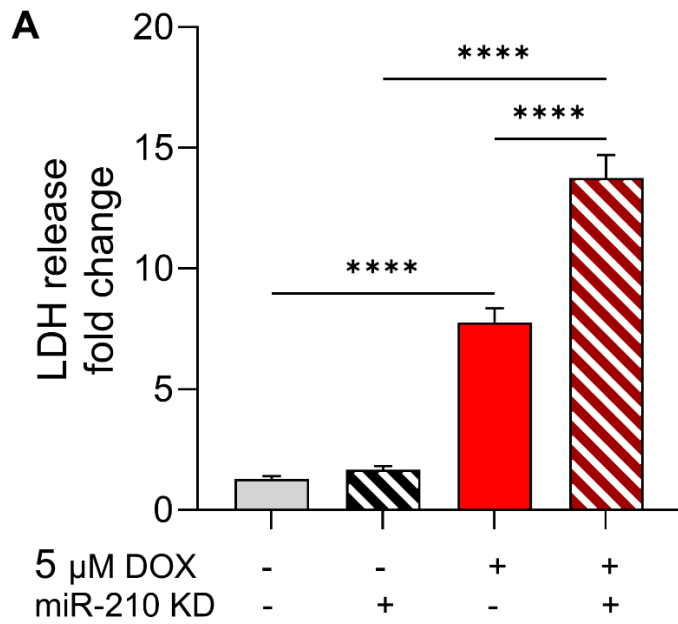
4.2 DOX dosage determination in hiPSC-CMs

After uncovering the protective effect of miR-210 on cell death in DOX-treated AC16 CMs, we wanted to further investigate the effects of DOX and miR-210 on electrophysiological properties in hiPSC-CMs using the MEA system. Given that the hiPSC-CMs are a different cell line than AC16 CMs, and that cell density and cell amount between a plated 48-well MEA plate and a plated 100 mm culture plate differ, we decided to perform a pilot study to determine the appropriate DOX concentration to use.

The concentrations chosen for the pilot study were 0.5 µM, 2 µM, 5 µM and 50 µM, as well as vehicle as control. The electrode activity was assessed over the course of 20 hours. The cells receiving 50 µM DOX were electrically inactive after 7 hours (data not shown). In the 5 µM DOX group, the loss of active electrodes was less obvious compared to the 50 µM DOX group, and more of a steady decline was observed. After 19 hours of DOX exposure, we observed a significant loss of active electrodes in the cells receiving 5 µM DOX compared to cells receiving 2 µM DOX ($p < 0.001$), as well as compared to cells receiving 0.5 µM DOX or vehicle ($p < 0.0001$). In the 2 µM DOX group, a significant loss of active electrodes was seen after 20 hours compared to cells treated with 0,5 µM DOX ($p < 0.05$). The cells receiving 0.5 µM DOX or vehicle were not affected (figure 5A).

To further examine if there was middle ground between the effect seen in the 2 µM group compared to the control group, we decided to treat three control wells with 1 µM DOX. The loss of electrodes was significantly greater in cells treated with 1 µM DOX compared to 0.5 µM DOX after 20 hours of DOX exposure ($p < 0.05$). The loss of electrodes appeared less in cells receiving 1 µM DOX compared to 2 µM DOX, but the difference was not statistically significant (figure 5B).

Based on the results of the pilot study, we decided to use 1 µM DOX for the main experiment. We feared that using 2 µM DOX or higher would reduce the amount and quality of the electrophysiological data from the experiment, and that any protective effect miR-210-3p might have would not be detected.

All references to DOX from here on will be with 1 µM concentration. Furthermore, due to the protective effect of miR-210 on cell death that was shown in AC16 CMs, we decided to only transfect the cells with miR-210-3p mimic, hereafter only referred to as miR-210. Transfection with no known complementarity to a human sequence (scramble) together with vehicle treatment was defined as control.
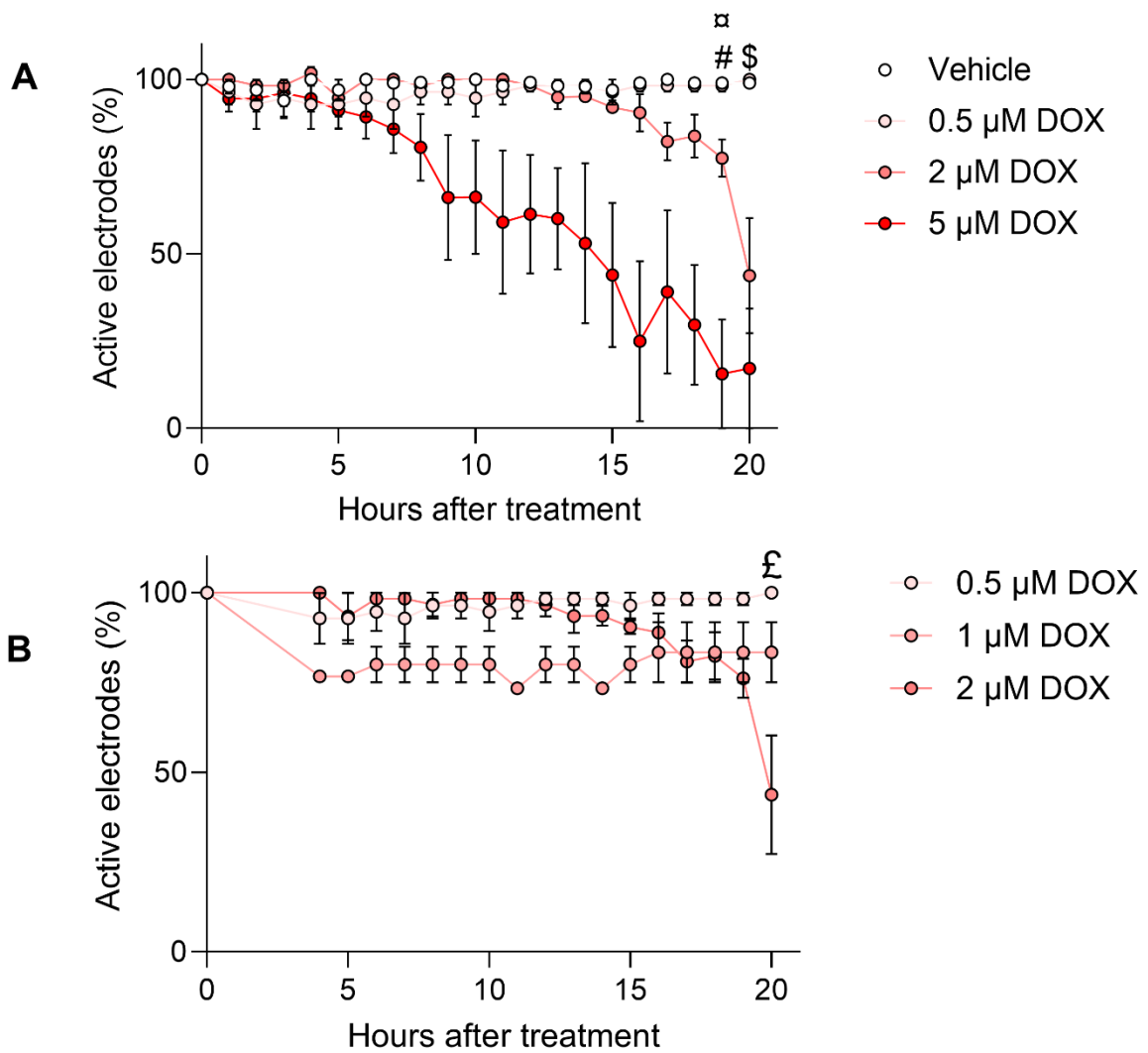
Figure 5: Active electrodes after DOX addition (A) and active electrodes after 1 µM DOX addition (B) in hiPSC-CMs. In figure 5B, the data on 0.5 µM and 2 µM are overlayed from the previous recording for comparison. The data is presented as the mean ± SEM. SEM: Standard error of the mean, vehicle: Sterile water, hiPSC-CMs: Human induced pluripotent stem cell cardiomyocytes. DOX: Doxorubicin. n is reported from baseline. Vehicle: n=7. 0.5 µM DOX: n=4. 1 µM DOX: n=3. 2 µM DOX: n=4. 5 µM DOX: n=4. Statistics were performed with a one-way ANOVA, with Tukey's multiple comparisons test.

¤ = $p < 0.001$ for 5 µM DOX vs. 2 µM DOX after 19 hours of treatment.

= $p < 0.0001$ for vehicle vs. 5 µM DOX and 0.5 µM DOX vs. 5 µM DOX after 19 hours of treatment.

$ = $p < 0.05$ for 2 µM DOX vs. 0.5 µM DOX after 20 hours of treatment

£ = $p < 0.05$ for 0.5 µM DOX vs. 1 µM DOX after 20 hours of treatment.

4.3 miR-210 attenuates cell death in DOX-treated hiPSC-CMs

To assess the levels of DOX-induced toxicity in hiPSC-CMS, we performed an LDH assay. The media used for the LDH assay was harvested 23 hours after DOX treatment.

In scramble-transfected cells, DOX treatment caused a significant increase in LDH release compared to vehicle ($p < 0.0001$). In DOX-treated cells, transfection with miR-210 significantly attenuated the LDH release compared to scramble ($p < 0.0001$) (figure 6A). This recapitulates the findings in the AC16 CMs.

To assess miR-210 levels, RT-qPCR was performed on cell lysate collected after the washout. In DOX-treated cells, transfection with miR-210 significantly increased the level of miR-210 compared to scramble ($p < 0.01$) (figure 6B).
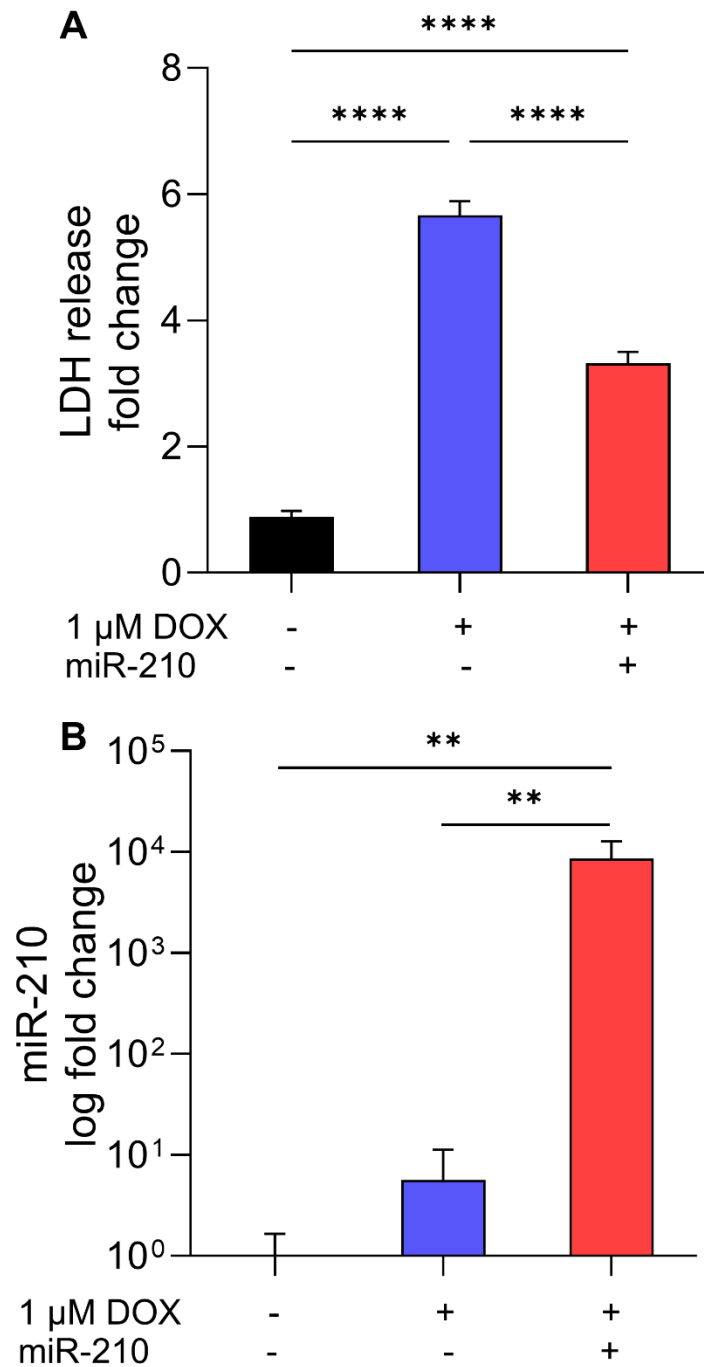
Figure 6: LDH release fold change (A) and miR-210 log fold change (B) in hiPSC-CMs transfected with scramble or miR-210 and treated with either DOX or vehicle. The data is presented as the mean ± SEM. SEM: Standard error of the mean, vehicle: Sterile water, DOX: Doxorubicin, miR-210: MicroRNA-210, LDH: Lactate dehydrogenase, hiPSC-CMs: Human induced pluripotent stem cell cardiomyocytes. LDH assay: n=4 for all groups. miR-210 rt-qPCR: n=3 for all groups. Statistics were performed with a one-way ANOVA, with Tukey's multiple comparisons test. ** = p < 0.01, **** = p < 0.0001.

4.4 Effects on active electrodes and beat period

To compare the number of electrophysiologically active cells between the groups, we measured the number of active electrodes. Comparing scramble-transfected cells,

treatment with DOX compared to vehicle did not reduce the number of active electrodes after 23 hours of treatment. However, 23 hours after washout, we found a significant loss of active electrodes in DOX-treated cells ($p < 0.0001$).

Comparing DOX-treated cells, we found a significant loss of active electrodes in cells transfected with miR-210 compared to scramble after 23 hours of treatment ($p < 0.05$) and 23 hours following washout ($p < 0.05$).

In comparison to control, DOX-treated cells transfected with miR-210 displayed a significant loss of active electrodes 23 hours after DOX treatment ($p < 0.001$) and 23 hours following washout ($p < 0.0001$) (figure 7A).

We examined the beat period to investigate temporal differences in the interval between beats. Comparing scramble-transfected cells, we observed no significant difference after 23 hours of DOX treatment. However, after 17 hours of washout, the beat period was significantly decreased in DOX-treated cells ($p < 0.001$). After 20 hours of washout, however, no difference was observed.

In DOX-treated cells, we did not find any difference between groups after 23 hours of DOX treatment or 17 hours following washout. After 20 hours of washout, however, there was a significant decrease in beat period in cells transfected with miR-210 compared to scramble ($p < 0.05$).

Compared to control, DOX-treated cells transfected with miR-210 displayed a significant increase in beat period after 23 hours of DOX treatment ($p < 0.01$), and a significant decrease in beat period after 17 hours of washout ($p < 0.0001$) and after 20 hours of washout ($p < 0.05$) (figure 7B).

After 20 hours of washout, there were fewer than three wells still electrically active. Because of the paucity of electrophysiological data, we elected not to include this data in the analysis. No data is displayed from here on when there are fewer than three electrically active wells in a given group.
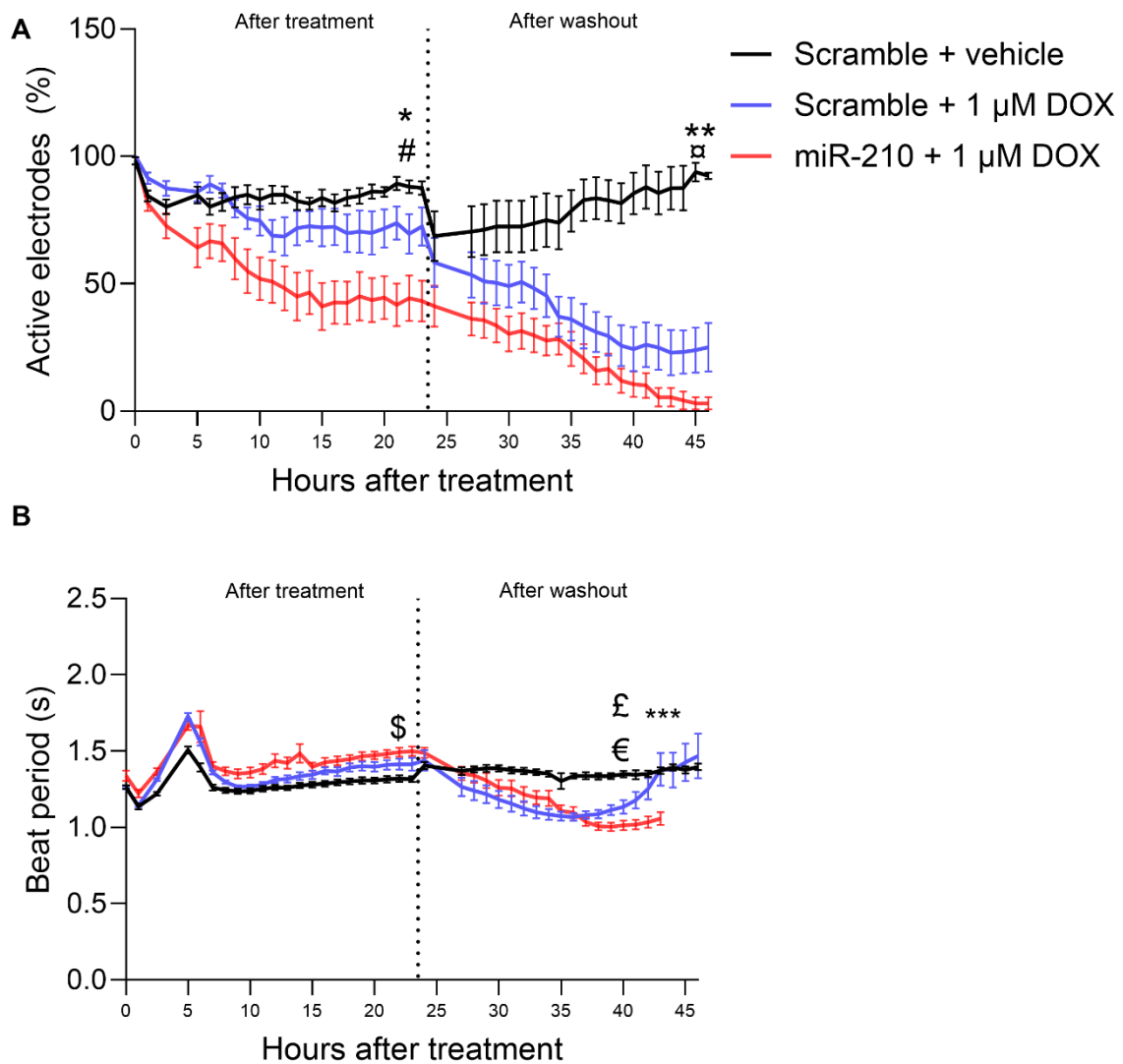
Figure 7: Active electrodes (A) and beat period (B) in hiPSC-CMs transfected with scramble or miR-210 and treated with either DOX or vehicle. The data is presented as the mean ± SEM. SEM: Standard error of the mean, miR-210: MicroRNA-210, DOX: Doxorubicin, vehicle: Sterile water. n=12 for all groups at baseline. Timepoints with n<3 were removed from analysis. Statistics were performed with a one-way ANOVA, with Tukey's multiple comparisons test. Scramble + vehicle is defined as control.

= $p < 0.001$ for miR-210 + DOX vs. control 23 hours after treatment.

* = $p < 0.05$ for miR-210 + DOX vs. scramble + DOX 23 hours after treatment.

¤ = $p < 0.0001$ for scramble + DOX vs. control and miR-210 + DOX vs. control 23 hours after washout.

** = $p < 0.05$ for miR-210 + DOX vs. scramble + DOX 23 hours after washout.

$ = $p < 0.01$ for miR210 + DOX vs. control 23 hours after treatment.

£ = $p < 0.001$ for scramble + DOX vs. control 17 hours after washout.

€ = $p < 0.0001$ for miR-210 + DOX vs. control 17 hours after washout.

*** = $p < 0.05$ for miR-210 + DOX vs. control and for miR-210 + DOX vs. scramble + DOX 20 hours after washout.

4.5 DOX and miR-210 affects field potential duration and depolarization characteristics

To assess the effects of DOX and miR-210 on electrophysiological properties, focusing on the duration of depolarization to repolarization, we examined FPD, spike amplitude, spike slope and APD.

4.5.1 DOX combined with miR-210 decreases FPD after washout

In examining FPD, we found no significant difference between any of the groups after 23 hours of DOX treatment, nor did we find a difference between scramble-transfected cells treated with DOX compared to vehicle after washout.

Comparing DOX-treated cells, we found a significant decrease 15 hours after washout in cells transfected with miR-210 compared to scramble (p < 0.05). Compared to control, DOX-treated cells transfected with miR-210 had a significant decrease in FPD 15 hours after washout (p < 0.05) (figure 8). This may indicate that miR-210 is involved in shortening FPD in DOX-treated cells.
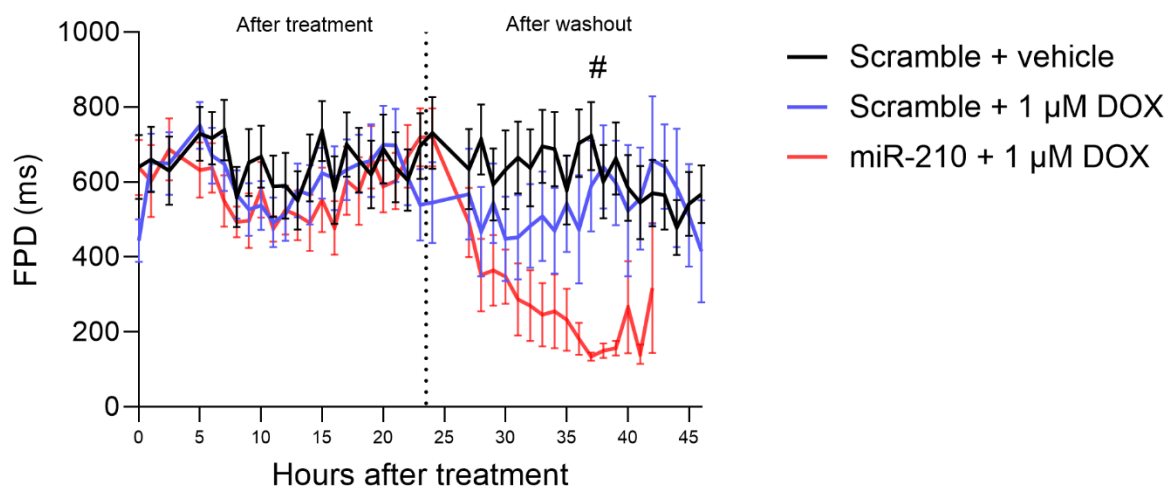
Figure 8: FPD after DOX treatment in hiPSC-CMs transfected with scramble or miR-210 and treated with either DOX or vehicle. The data is presented as the mean ± SEM. SEM: Standard error of the mean, miR-210: MicroRNA-210, DOX: Doxorubicin, vehicle: Sterile water, FPD: Field potential duration. Parentheses signify wells yet to be treated with vehicle or DOX. n=12 for all groups at baseline. Timepoints with n<3 were removed from analysis. Statistics were performed with a one-way ANOVA, with Tukey's multiple comparisons test. Scramble + vehicle is defined as control.
= p < 0.05 for miR-210 + DOX vs. both scramble + DOX and control 15 hours after washout.

4.5.2 DOX decreases spike amplitude and spike slope, regardless of miR-210 transfection status

To assess the effects on phase 1 of the action potential due to effects on voltage-gated sodium channels, we examined the spike amplitude and the spike slope.

After 23 hours of DOX treatment, no significant differences were found in spike amplitude between any of the groups. After 23 hours of washout, we found that when comparing scramble-transfected cells, DOX-treated cells had a significant decrease in spike amplitude compared to vehicle ($p < 0.0001$).

In DOX-treated cells, we found no difference between cells transfected with miR-210 compared to scramble after 23 hours of washout.

Compared to control, DOX-treated cells transfected with miR-210 had a significant decrease in spike amplitude 23 hours after washout ($p < 0.0001$) (figure 9A).

To compare how the speed of depolarization differed between the groups, we analyzed the spike slope. No significant differences between any of the groups were found after 23 hours of DOX treatment.

Comparing scramble-transfected cells, we found that DOX treatment significantly decreased the spike slope after 20 hours of washout compared to vehicle ($p < 0.001$).

No difference was found between DOX-treated cells transfected with miR-210 compared to scramble 20 hours following washout.

DOX-treated cells transfected with miR-210 were found to have a significant decrease in the spike slope 20 hours following washout ($p < 0.01$) (figure 9B).
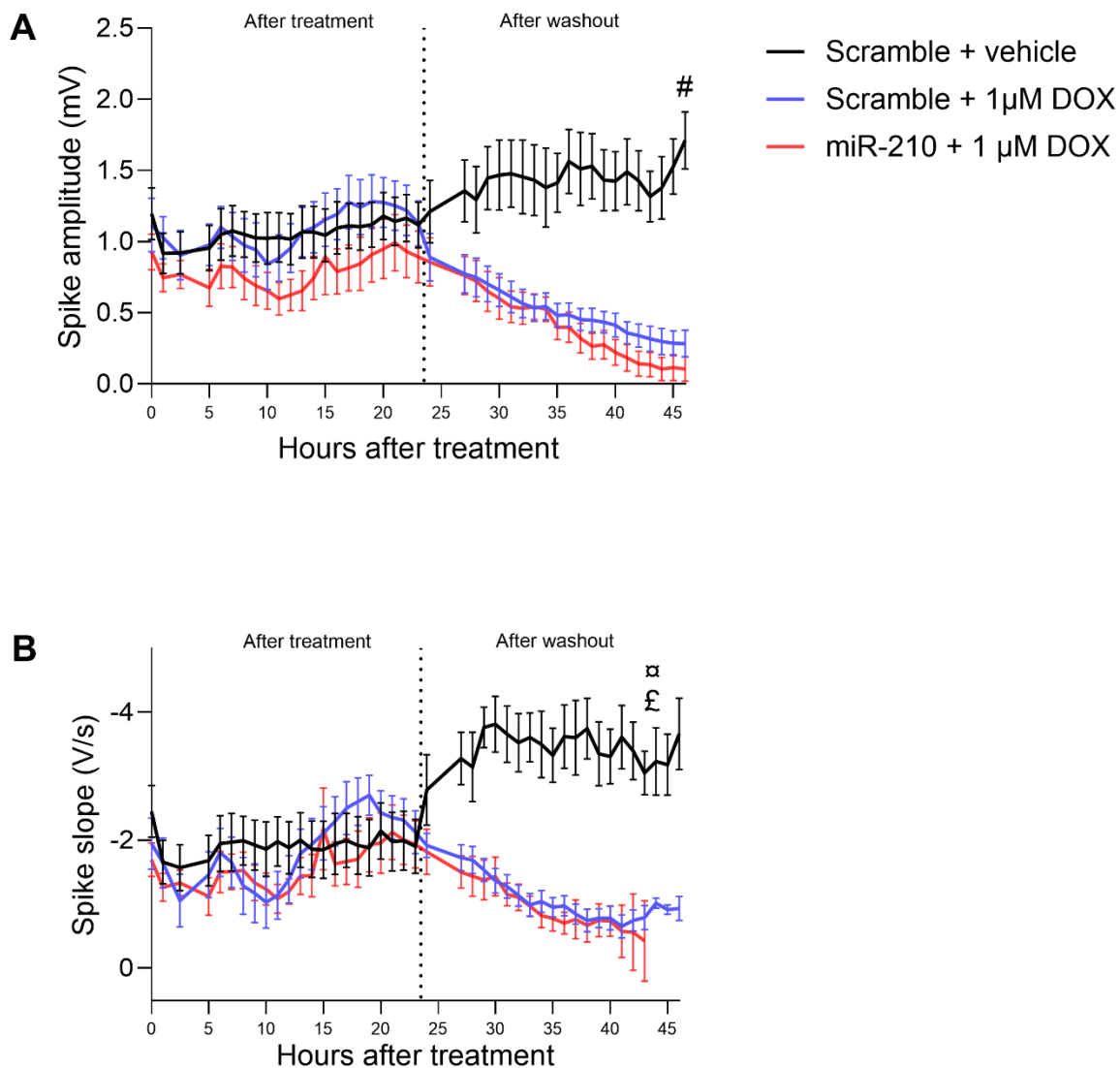
Figure 9: Spike amplitude (A) and spike slope (B) in hiPSC-CMs transfected with scramble or miR-210 and treated with either DOX or vehicle. The axis for figure 9B has been inverted. The data is presented as the mean ± SEM. SEM: Standard error of the mean, miR-210: MicroRNA-210, DOX: Doxorubicin, vehicle: Sterile water. n=12 for all groups at baseline. Timepoints with n<3 were removed from analysis. Statistics were performed with a one-way ANOVA, with Tukey's multiple comparisons test. Scramble + vehicle is defined as control.
= p < 0.0001 for control vs. both scramble + DOX and mir-210 + DOX after 23 hours of washout.
¤ = p < 0.001 for scramble + DOX vs. control after 20 hours of washout.
£ = p < 0.01 for miR-210 + DOX vs. control after 20 hours of washout.

4.5.3 Local extracellular action potential (LEAP)

To further investigate the electrical behavior at a more detailed level, we examined the LEAP. A manual selection of wells was done to capture a good LEAP signal. It was further analyzed to examine differences in repolarization kinetics, demonstrated by differences in action potential duration (APD). Compared to control, miR-210 + DOX showed a significantly greater delay in reaching 30% of the APD (APD 30) (p < 0.05) and 50% of the APD (APD 50) (p < 0.05). We found no significant difference between the groups in reaching 90% of the APD (APD 90) (figure 10).
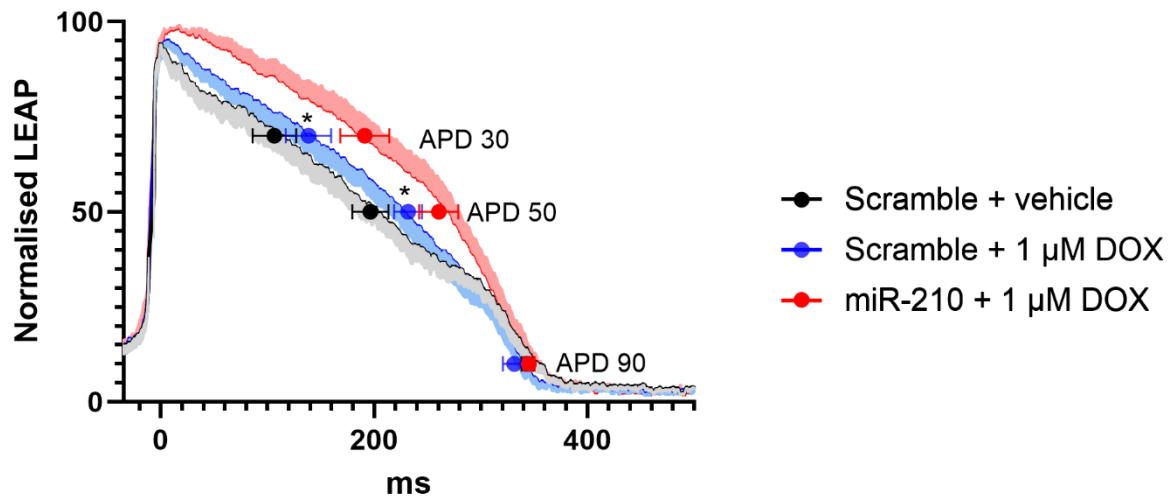
Figure 10: Averaged LEAP in hiPSC-CMs transfected with scramble or miR-210 and treated with either DOX or vehicle. The data is presented as the mean ± SEM. SEM: Standard error of the mean, vehicle: Sterile water, miR-210: MicroRNA-210-3P, DOX: Doxorubicin, APD 30: 30% of action potential duration, APD 50: 50% of action potential duration, APD 90: 90% of action potential duration. Scramble + vehicle: n=7 for all APD timepoints. Scramble + DOX: n=7 for all APD timepoints. miR-210 + DOX: n=5 for APD 30 and APD 50, n=6 for APD 90. Statistics were performed with a one-way ANOVA, with Tukey's multiple comparisons test. Scramble + vehicle is defined as control.

* = $p < 0.05$ for miR-210 + DOX vs. control.

5 Discussion

5.1 miR-210 protects against cell death, and DOX induces upregulation of miR-210

In the present study, using the LDH assay, we found that DOX induces cell death in both AC16 CMs and hiPSC-CMs when exposed to 5 µM and 1 µM DOX, respectively. These findings mirror what is already known about the general cytotoxic characteristics of DOX (62, 63). By using the miR-210 hybridization assay and RT-qPCR, we confirmed that higher levels of miR-210 are associated with lower amounts of LDH release in both cell lines.

In the AC16 cell line, DOX treatment significantly increased the LDH release in EV-transfected cells compared to vehicle. When transfecting with miR-210 OE, we found that the increase in LDH release in DOX-treated cells was attenuated compared to cells transfected with scramble. This finding indicates that miR-210 reduces the amount of cell death in DOX-treated AC16 CMs. Repeating the experiment using miR-210 KD instead of miR-210 OE, we again found that DOX treatment increased LDH release in EV-transfected cells compared to vehicle, but transfection with miR-210 KD significantly increased the LDH release in DOX-treated cells compared to transfection with EV, contrasting our findings when transfecting with miR-210 OE, and solidifying miR-210's ability to protect against DOX-induced cell death.

In the hiPSC-CMs, we observed the same protective effects of miR-210 as seen in the AC16 CMs. Treatment with DOX in EV-transfected cells led to an increase in LDH release, while transfection with miR-210 attenuated the LDH release in DOX-treated cells, as confirmed by RT-qPCR.

While miR-210 has been shown to protect against cell death in cells exposed to hypoxia, MI and IR injury (49, 50, 53, 54), we are, to our knowledge, the first to show in vitro evidence of miR-210's attenuation of DOX-induced cell death. Given our findings in the DOX-treated AC16 CMs, where increased levels of miR-210 attenuated LDH release, and decreased levels of miR-210 exacerbated LDH release, as well as the replication of the attenuation of LDH release in DOX-treated hiPSC-CMs transfected with miR-210, this is strong evidence for the pivotal role miR-210 has in preventing DOX-induced cell death in CMs.

While miR-210 appears to protect against DOX-induced cell death in vitro, given that DOX is used to treat cancer patients, the effects of miR-210 on cancer cells are important to consider. A meta-analysis by Wang et al. examined the link between miR-210 levels, either from blood samples or tissue samples, and prognosis in cancer patients. While the authors found that miR-210 was downregulated in a few cancer types, upregulation of miR-210 was more common, seen in breast cancer, colon cancer and ovarian cancer, among others. The upregulation of miR-210 was positively correlated with a poor prognosis (64).

In cancer, the area in which the tumor resides often becomes hypoxic due to the accelerated pace of growth of malignant cells compared to normal cells (65). As

mentioned before, hypoxia upregulates transcription of miR-210 through binding of HIF-1α to hypoxia-responsive elements on the promoter of the miR-210 gene (66). This has been shown to affect cancer progression in several ways (67). In angiogenesis, the proteins ephrin-A3 (EFNA3) and protein tyrosine phosphatase 1B (PTP1B) are important for negative regulation of angiogenic signaling pathways by interacting with vascular endothelial growth factor receptor 2 and Eph receptors. miR-210 inhibits both EFNA3 and PTP1B, thereby improving the vascular supply to the cancerous cells, providing both nutrients and gases, as well as an opportunity to metastasize (51, 67). In the mitochondria, miR-210 plays a part in causing a metabolic shift to aerobic glycolysis through affecting the electron transport chain by inhibiting iron-sulfur clusters (ISCU) 1/2 (68). This metabolic shift is known as the Warburg effect, and is associated with tumor progression (69). Lastly, miR-210 inhibits apoptosis by downregulating several proteins, an example of which is CASP8AP2, as previously mentioned. The inhibitory effect on apoptosis in malignant cells can further drive tumor development (67). Given the conflicting roles miR-210 has in CMs and malignant cells, clinical translation might prove challenging.

Through our experiments, we also found that DOX itself upregulated miR-210 levels. By using the miR-210 hybridization assay, we found that DOX treatment itself induces an increase in miR-210 levels in AC16 CMs transfected with EV in both the OE and the KD experiment. It is known that DOX induces transcriptional changes in CMs (70), and the upregulation of miR-210 could be an adaptive response to protect the cells from DOX-induced cardiotoxicity.

To put our findings in a broader perspective, a meta-analysis by Pereira et al. found a downregulation of miR-210 in breast cancer patient with signs of cardiotoxicity after treatment with epirubicin or DOX, as compared to patients who received anthracycline treatment with no signs of cardiotoxicity (71). Because of the relatively lower levels of miR-210 in these patients, the authors argue for the possible benefit in examining a cluster of different miRNAs to identify patients who will develop cardiotoxic side effects. This viewpoint is echoed by Rosenfeld et al., but they add that any dysregulation of miRNA levels could represent an adaptive state (72). While altering miR-210 levels therapeutically might not halt the development of cardiotoxicity, miR-210 could nevertheless serve as a useful biomarker for identifying patients more likely to develop cardiotoxicity.

It is worth noting that in the meta-analysis by Pereira et al., blood samples were taken before treatment with DOX (73), thus differing from our experimental setup, where miR-210 levels were assessed after DOX treatment and in an in vitro model using cell lysate. Additionally, there could be differences between miRNA levels in tissue versus body fluids, making it difficult to compare findings between in vitro and in vivo studies. A positive correlation has been shown between miRNA levels in plasma/serum and cardiac tissue (74), but these are global miRNA findings, and such a correlation might not hold true for miR-210.

While we observed an increase in miR-210 levels in EV-transfected AC16 CMs treated with DOX, we found no such increase in the DOX-treated hiPSC-CMs transfected with scramble. This could have several explanations. Firstly, the DOX dosage between the experiments differed. In the AC16 CMs, we chose 5 µM DOX, whereas we elected to treat with 1 µM DOX in the hiPSC-CMs. When plating the AC16 CMs, we used 100 mm culture dishes, and the DOX treatment took place when the culture dishes were approximately

90% confluent. At full confluency, the number of cells in a 100 mm culture dish is approximately 8 million cells (75). For the hiPSC-CMs, approximately 50 000 cells were used in plating, topping off the wells with 300 µL of MM. There was thus a difference in cell density between the different experiments. The difference in DOX dosage relative to cell density might explain why we did not observe a significant increase in miR-210 in DOX-treated hiPSC-CMs transfected with scramble. Additionally, the limited experience of the investigator doing the RT-qPCR to quantify the miR-210 amount could have played a role. Inaccurate pipetting is a significant source of error when doing RT-qPCR (76), and could have led to large variation in miR-210 levels between the groups. Lastly, only three samples were used in each experimental group. Combined with the large variation in miR-210 levels, the small sample size could have made it difficult to detect a significant difference.

5.2 DOX and miR-210 alter electrophysiological properties

To first illustrate the effect of DOX and miR-210 on a general level, we will first examine the changes in active electrodes between the experimental groups.

Firstly, after washout, we found that the percentage of active electrodes went down in all groups, indicating that media change was a significant stressor for the cells. While the control group recuperated after the media change, the percentage of active electrodes continued to drop in both groups receiving DOX, continuing the trend seen before washout. As seen in other electrophysiological measurements, the number of wells outputting data after washout were markedly reduced in the DOX-treated cells, and particularly in DOX-treated cells transfected with miR-210.

As expected, due to its effects on cell death, DOX treatment led to a loss of active electrodes compared to vehicle. Interestingly, while transfection with miR-210 protected against cell death, it also led to a loss of active electrodes in DOX-treated cells compared to transfection with scramble. The loss of active electrodes in DOX-treated cells transfected with miR-210 was seen earlier, indicating a faster loss of contractile function due to miR-210. One possible mechanism explaining this might be miR-210's effects on the mitochondria.

ATP production is vital for proper contractile function of the heart. In fact, around 30% of the total volume of a cardiomyocyte is made up of mitochondria. Around 60% of the ATP is directly used by the ATPase vital for actin-myosin interaction, while the rest is used for maintaining ion balance, for instance by SERCA to maintain proper calcium balance. In healthy cardiac tissue, oxidative phosphorylation is the main metabolic pathway through which ATP is generated, while aerobic glycolysis is a less important contributor (77). If ATP production were to go down, this could likely have deleterious effects on cardiac contractile ability. As shown previously, miR-210 downregulates mitochondrial function and oxidative phosphorylation through ISCU1/2 inhibition (78). This downregulation could affect the energy available for maintaining contractile ability by reducing ATP production. As we have shown in our study, while treatment with DOX alone significantly reduces the number of active electrodes, addition of miR-210 both accelerates and exacerbates this reduction. To further examine the causes of this, the bioenergetics of CMs treated with DOX and transfected with miR-210 should be studied.

Further exploring electrophysiological properties on a general level, we looked at the beat period. We found a decrease in beat period after DOX treatment in scramble-transfected cells, but the beat period was again no different from control after the washout period was complete. This could indicate that the cells were able to recuperate upon replacement of the media. Interestingly, DOX-treated cells transfected with miR-210 showed a pattern of beat period reversal. After DOX treatment, the beat period was significantly increased, but after the washout period was complete, the beat period was significantly reduced compared to control. When analyzing the FPD, we again found that the combination of DOX and miR-210 significantly altered the electrophysiology. We observed a significant shortening of the FPD in DOX-treated cells transfected with miR-210 compared to both control and scramble-transfected cells. It is known that that the FPD and the beat rate have an interdependent relationship (79), and consequently FPD and the beat period should also be linked. The decrease in FPD would which is in line with our findings.

Upon a closer examination of the depolarization characteristics, we found a decrease in spike amplitude and spike slope in DOX-treated cells compared to control, regardless of miR-210 transfection status. As mentioned previously, ROS generation can affect the Nav1.5 voltage-gated sodium channel through a suppression of SCN5a transcription (23). Since DOX has been shown to decrease the depolarization spike velocity (21), which is supported through our findings as well, ROS generation could explain the decrease in both magnitude and speed of the depolarization that we found in our study. The ROS generation due to DOX exposure could have been too large to be attenuated by miR-210, thus explaining miR-210's lack of protective effect in the DOX-treated cells, but further studies would be needed to verify this.

Furthermore, we analyzed the repolarization kinetics by examining the APD. Here we again found a significant difference between cells receiving DOX and miR-210 compared to control. DOX-treated cells transfected with miR-210 were delayed in reaching APD 30 and APD 50, but there was no difference between the groups in reaching APD 90. Through ROS generation, DOX has been shown to increase SERCA inhibition and increase RyR activity (24), as well as inhibiting voltage-gated potassium channels (26), which could have an effect on APD. We observed no difference between cells treated with DOX alone compared to control, thus implying an effect of miR-210. Since miR-210 decreases ROS generation (52), it seems unlikely that the observed delay in APD 30 and APD 50 would be due to transfection with miR-210 in DOX-treated cells. Though there was no difference in APD 90, indicating no alteration in total APD between the groups, further studies using patch clamp techniques could elucidate precisely which ion channels are involved, and if miR-210 affects APD on its own.

Altering the function of cardiac ion channels can lead to the development of arrythmias (22). As we observed in our study, DOX and miR-210 affect the electrophysiological properties of hiPSC-CMs, possibly giving rise to arrhythmia. A recently published meta-analysis by Dean et al. looked at the arrhythmogenic properties of anthracyclines and concluded that these compounds do indeed increase the risk of arrhythmia. Consequently, the authors cautioned against the use of these drugs in susceptible patients, as well as encouraging screening before receiving treatment (80).

6 Limitations and future perspectives

Our study has several limitations. Firstly, with regards to the comparability between the two cell lines, the change in miR-210 levels were vastly different between the AC16 CMs and the hiPSC-CMs. In the AC16 CMs, the fold change was <10 in cells transfected with miR-210 OE. In the hiPSC-CMs, however, the fold change was around 10,000 in cells treated with miR-210 mimic. This difference in magnitude makes it hard to compare the experiments, and if such a comparison between cell lines should be made, future research should standardize the miR-210 dosage. Secondly, because of different plating parameters for AC16 CMs and hiPSC-CMs, the DOX dosage had to be altered. With different dosages of DOX, this further complicates the comparability of the findings in the two cell lines. Thirdly, we also used a miR-210 KD in the AC16 CMs, while this was not done in the hiPSC-CMs. Because this would lower the sample size if we were to have also transfected the cells with miR-210 KD, we elected not to do this. To further validate the effects miR-210 has on cell death in the hiPSC-CMs, future research should also include miR-210 KD.

In the pilot experiment to determine the DOX dosage, we chose to test five different DOX concentrations. In retrospect, given the small sample size in each group, we should have chosen fewer concentrations to gain statistical power, preferably omitting both 50 µM and 5 µM DOX, as we suspected that these concentrations would probably cause major cell death in a short period of time because of the cell density in the hiPSC-CMs. Even though including these concentrations gave us verification of the cytotoxic effect of DOX, with a larger sample size we could have had more data to more accurately pick an appropriate DOX concentration for the main experiment, possibly giving us better electrophysiological data from out experiment.

While collected data on cell death through the LDH assay, we did not examine which pathways of cell death were affected. As mentioned previously, DOX can affect cell death through many different pathways (14). We showed that miR-210 attenuates DOX-induced cell death, and future experiments should elucidate exactly which pathways are affected to gain a more thorough understanding of miR-210's function in this regard.

7 Conclusion

This study looked at the effects of DOX and miR-210 on cell death and electrophysiological properties in AC16 CMs and hiPSC-CMs. Our aims were to elucidate the effect of DOX and miR-210 on cell death in AC16 CMs and hiPSC-CMs, and to characterize the electrophysiological effects of DOX and miR-210 in hiPSC-CMs.

We demonstrated that DOX induces cell death in both cell lines by using LDH release as a marker for cell death, a finding which is consistent with previous work, and that miR-210 significantly attenuated DOX-induced cell death. In AC16 CMs, overexpressing and knocking down miR-210 led to attenuation and exacerbation of DOX-induced cell death, respectively. In hiPSC-CMs, transfection with a miR-210 mimic significantly attenuated DOX-induced cell death.

Electrophysiological assessment revealed significant alterations in DOX-treated cells. The number of active electrodes able to detect beats were significantly reduced by DOX, and miR-210 appeared to exacerbate this. Additional electrophysiological parameters were also affected, notably the beat period, FPD, spike amplitude and spike slope. Simultaneous transfection with miR-210 did not change the reduction seen in spike amplitude and spike slope but was associated with a shortening of the FPD and an alteration of the beat period.

While our findings on cell death suggest that miR-210 has a protective role on cell death in cells treated with DOX, the effects seen on electrophysiological parameters warrant further study to elucidate which mechanisms are at play. Future research should investigate the specific effects of miR-210 on electrophysiological properties of CMs to further explore the potential therapeutic benefit of miR-210 as a cardioprotective agent.

References

1. Roth GA, Mensah GA, Johnson CO, Addolorato G, Ammirati E, Baddour LM, et al. Global Burden of Cardiovascular Diseases and Risk Factors, 1990-2019: Update From the GBD 2019 Study. J Am Coll Cardiol. 2020;76(25):2982-3021.
2. Bray F, Laversanne M, Weiderpass E, Soerjomataram I. The ever-increasing importance of cancer as a leading cause of premature death worldwide. Cancer. 2021;127(16):3029-30.
3. Olvera Lopez E, Ballard BD, Jan A. Cardiovascular Disease. [Updated 2023 Aug 22]. In: StatPearls [Internet]. Treasure Island (FL): StatPearls Publishing; 2023 Jan-. Available from: https://www.ncbi.nlm.nih.gov/books/NBK535419/.
4. Bays HE, Kulkarni A, German C, Satish P, Iluyomade A, Dudum R, et al. Ten things to know about ten cardiovascular disease risk factors - 2022. Am J Prev Cardiol. 2022;10:100342.
5. Mladěnka P, Applová L, Patočka J, Costa VM, Remiao F, Pourová J, et al. Comprehensive review of cardiovascular toxicity of drugs and related agents. Med Res Rev. 2018;38(4):1332-403.
6. Broder H, Gottlieb RA, Lepor NE. Chemotherapy and cardiotoxicity. Rev Cardiovasc Med. 2008;9(2):75-83.
7. Amjad MT, Chidharla A, Kasi A. Cancer Chemotherapy. [Updated 2023 Feb 27]. In: StatPearls [Internet]. Treasure Island (FL): StatPearls Publishing; 2023 Jan-. Available from: https://www.ncbi.nlm.nih.gov/books/NBK564367/.
8. Pearce A, Haas M, Viney R, Pearson SA, Haywood P, Brown C, et al. Incidence and severity of self-reported chemotherapy side effects in routine care: A prospective cohort study. PLoS One. 2017;12(10):e0184360.
9. Volkova M, Russell R, 3rd. Anthracycline cardiotoxicity: prevalence, pathogenesis and treatment. Curr Cardiol Rev. 2011;7(4):214-20.
10. Carvalho FS, Burgeiro A, Garcia R, Moreno AJ, Carvalho RA, Oliveira PJ. Doxorubicin-induced cardiotoxicity: from bioenergetic failure and cell death to cardiomyopathy. Med Res Rev. 2014;34(1):106-35.
11. Takemura G, Fujiwara H. Doxorubicin-induced cardiomyopathy from the cardiotoxic mechanisms to management. Prog Cardiovasc Dis. 2007;49(5):330-52.
12. Chatterjee K, Zhang J, Honbo N, Karliner JS. Doxorubicin cardiomyopathy. Cardiology. 2010;115(2):155-62.
13. McGowan JV, Chung R, Maulik A, Piotrowska I, Walker JM, Yellon DM. Anthracycline Chemotherapy and Cardiotoxicity. Cardiovasc Drugs Ther. 2017;31(1):63-75.
14. Kciuk M, Gielecińska A, Mujwar S, Kołat D, Kałuzińska-Kołat Ż, Celik I, et al. Doxorubicin-An Agent with Multiple Mechanisms of Anticancer Activity. Cells. 2023;12(4).
15. Rawat PS, Jaiswal A, Khurana A, Bhatti JS, Navik U. Doxorubicin-induced cardiotoxicity: An update on the molecular mechanism and novel therapeutic strategies for effective management. Biomedicine & Pharmacotherapy. 2021;139:111708.
16. Wenningmann N, Knapp M, Ande A, Vaidya TR, Ait-Oudhia S. Insights into Doxorubicin-induced Cardiotoxicity: Molecular Mechanisms, Preventive Strategies, and Early Monitoring. Mol Pharmacol. 2019;96(2):219-32.
17. Shi S, Chen Y, Luo Z, Nie G, Dai Y. Role of oxidative stress and inflammation-related signaling pathways in doxorubicin-induced cardiomyopathy. Cell Communication and Signaling. 2023;21(1):61.
18. Jiang X, Wang X. Cytochrome C-Mediated Apoptosis. Annual Review of Biochemistry. 2004;73(Volume 73, 2004):87-106.
19. Hashimoto N, Nagano H, Tanaka T. The role of tumor suppressor p53 in metabolism and energy regulation, and its implication in cancer and lifestyle-related diseases. Endocr J. 2019;66(6):485-96.

20.   Giglia-Mari G, Zotter A, Vermeulen W. DNA damage response. Cold Spring Harb Perspect Biol. 2011;3(1):a000745.
21.   Benjanuwattra J, Siri-Angkul N, Chattipakorn SC, Chattipakorn N. Doxorubicin and its proarrhythmic effects: A comprehensive review of the evidence from experimental and clinical studies. Pharmacol Res. 2020;151:104542.
22.   Grant AO. Cardiac Ion Channels. Circulation: Arrhythmia and Electrophysiology. 2009;2(2):185-94.
23.   Mao W, You T, Ye B, Li X, Dong HH, Hill JA, et al. Reactive oxygen species suppress cardiac NaV1.5 expression through Foxo1. PLoS One. 2012;7(2):e32738.
24.   Shinlapawittayatorn K, Chattipakorn SC, Chattipakorn N. The effects of doxorubicin on cardiac calcium homeostasis and contractile function. J Cardiol. 2022;80(2):125-32.
25.   De Nicolo B, Cataldi-Stagetti E, Diquigiovanni C, Bonora E. Calcium and Reactive Oxygen Species Signaling Interplays in Cardiac Physiology and Pathologies. Antioxidants (Basel). 2023;12(2).
26.   Strigli A, Raab C, Hessler S, Huth T, Schuldt AJT, Alzheimer C, et al. Doxorubicin induces caspase-mediated proteolysis of KV7.1. Communications Biology. 2018;1(1):155.
27.   Hellenkamp K, Nolte K, von Haehling S. Pharmacological treatment options for heart failure with reduced ejection fraction: A 2022 update. Expert Opin Pharmacother. 2022;23(6):673-80.
28.   Bansal N, Adams MJ, Ganatra S, Colan SD, Aggarwal S, Steiner R, et al. Strategies to prevent anthracycline-induced cardiotoxicity in cancer survivors. Cardio-Oncology. 2019;5(1):18.
29.   Schroeder PE, Hasinoff BB. The doxorubicin-cardioprotective drug dexrazoxane undergoes metabolism in the rat to its metal ion-chelating form ADR-925. Cancer Chemotherapy and Pharmacology. 2002;50(6):509-13.
30.   Lyu YL, Kerrigan JE, Lin C-P, Azarova AM, Tsai Y-C, Ban Y, et al. Topoisomerase IIβ–Mediated DNA Double-Strand Breaks: Implications in Doxorubicin Cardiotoxicity and Prevention by Dexrazoxane. Cancer Research. 2007;67(18):8839-46.
31.   Vejpongsa P, Yeh ETH. Prevention of Anthracycline-Induced Cardiotoxicity: Challenges and Opportunities. Journal of the American College of Cardiology. 2014;64(9):938-45.
32.   Tebbi CK, London WB, Friedman D, Villaluna D, Alarcon PAD, Constine LS, et al. Dexrazoxane-Associated Risk for Acute Myeloid Leukemia/Myelodysplastic Syndrome and Other Secondary Malignancies in Pediatric Hodgkin's Disease. Journal of Clinical Oncology. 2007;25(5):493-500.
33.   Macedo AVS, Hajjar LA, Lyon AR, Nascimento BR, Putzu A, Rossi L, et al. Efficacy of Dexrazoxane in Preventing Anthracycline Cardiotoxicity in Breast Cancer. JACC CardioOncol. 2019;1(1):68-79.
34.   Geisberg CA, Sawyer DB. Mechanisms of anthracycline cardiotoxicity and strategies to decrease cardiac damage. Curr Hypertens Rep. 2010;12(6):404-10.
35.   Ho PTB, Clark IM, Le LTT. MicroRNA-Based Diagnosis and Therapy. Int J Mol Sci. 2022;23(13).
36.   Romano G, Veneziano D, Acunzo M, Croce CM. Small non-coding RNA and cancer. Carcinogenesis. 2017;38(5):485-91.
37.   Çakmak HA, Demir M. MicroRNA and Cardiovascular Diseases. Balkan Med J. 2020;37(2):60-71.
38.   O'Brien J, Hayder H, Zayed Y, Peng C. Overview of MicroRNA Biogenesis, Mechanisms of Actions, and Circulation. Frontiers in Endocrinology. 2018;9.
39.   Gingras AC, Raught B, Sonenberg N. eIF4 initiation factors: effectors of mRNA recruitment to ribosomes and regulators of translation. Annu Rev Biochem. 1999;68:913-63.
40.   Sadakierska-Chudy A. MicroRNAs: Diverse Mechanisms of Action and Their Potential Applications as Cancer Epi-Therapeutics. Biomolecules. 2020;10(9).
41.   Zhang B, Pan X, Cobb GP, Anderson TA. microRNAs as oncogenes and tumor suppressors. Dev Biol. 2007;302(1):1-12.

42.	Ardekani AM, Naeini MM. The Role of MicroRNAs in Human Diseases. Avicenna J Med Biotechnol. 2010;2(4):161-79.

43.	Corsten MF, Dennert R, Jochems S, Kuznetsova T, Devaux Y, Hofstra L, et al. Circulating MicroRNA-208b and MicroRNA-499 reflect myocardial damage in cardiovascular disease. Circ Cardiovasc Genet. 2010;3(6):499-506.

44.	Wahlquist C, Jeong D, Rojas-Muñoz A, Kho C, Lee A, Mitsuyama S, et al. Inhibition of miR-25 improves cardiac contractility in the failing heart. Nature. 2014;508(7497):531-5.

45.	Hinkel R, Penzkofer D, Zühlke S, Fischer A, Husada W, Xu QF, et al. Inhibition of microRNA-92a protects against ischemia/reperfusion injury in a large-animal model. Circulation. 2013;128(10):1066-75.

46.	He J, Liu D, Zhao L, Zhou D, Rong J, Zhang L, et al. Myocardial ischemia/reperfusion injury: Mechanisms of injury and implications for management (Review). Exp Ther Med. 2022;23(6):430.

47.	Marwarha G, Røsand Ø, Scrimgeour N, Slagsvold KH, Høydal MA. miR-210 Regulates Apoptotic Cell Death during Cellular Hypoxia and Reoxygenation in a Diametrically Opposite Manner. Biomedicines. 2022;10(1):42.

48.	Chan YC, Banerjee J, Choi SY, Sen CK. miR-210: The Master Hypoxamir. Microcirculation. 2012;19(3):215-23.

49.	Kim HW, Haider HK, Jiang S, Ashraf M. Ischemic preconditioning augments survival of stem cells via miR-210 expression by targeting caspase-8-associated protein 2. J Biol Chem. 2009;284(48):33161-8.

50.	Marwarha G, Røsand Ø, Slagsvold KH, Høydal MA. GSK3β Inhibition Is the Molecular Pivot That Underlies the Mir-210-Induced Attenuation of Intrinsic Apoptosis Cascade during Hypoxia. Int J Mol Sci. 2022;23(16).

51.	Ivan M, Huang X. miR-210: fine-tuning the hypoxic response. Adv Exp Med Biol. 2014;772:205-27.

52.	Song R, Dasgupta C, Mulder C, Zhang L. MicroRNA-210 Controls Mitochondrial Metabolism and Protects Heart Function in Myocardial Infarction. Circulation. 2022;145(15):1140-53.

53.	Hu S, Huang M, Li Z, Jia F, Ghosh Z, Lijkwan MA, et al. MicroRNA-210 as a novel therapy for treatment of ischemic heart disease. Circulation. 2010;122(11 Suppl):S124-31.

54.	Arif M, Pandey R, Alam P, Jiang S, Sadayappan S, Paul A, et al. MicroRNA-210-mediated proliferation, survival, and angiogenesis promote cardiac repair post myocardial infarction in rodents. Journal of Molecular Medicine. 2017;95(12):1369-85.

55.	Davidson MM, Nesti C, Palenzuela L, Walker WF, Hernandez E, Protas L, et al. Novel cell lines derived from adult human ventricular cardiomyocytes. J Mol Cell Cardiol. 2005;39(1):133-47.

56.	Onódi Z, Visnovitz T, Kiss B, Hambalkó S, Koncz A, Ágg B, et al. Systematic transcriptomic and phenotypic characterization of human and murine cardiac myocyte cell lines and primary cardiomyocytes reveals serious limitations and low resemblances to adult cardiac phenotype. J Mol Cell Cardiol. 2022;165:19-30.

57.	Berg PC, Hansson Å ML, Røsand Ø, Marwarha G, Høydal MA. Overexpression of Neuron-Derived Orphan Receptor 1 (NOR-1) Rescues Cardiomyocytes from Cell Death and Improves Viability after Doxorubicin Induced Stress. Biomedicines. 2021;9(9).

58.	Kumar P, Nagarajan A, Uchil PD. Analysis of Cell Viability by the Lactate Dehydrogenase Assay. Cold Spring Harb Protoc. 2018;2018(6).

59.	Kielkopf CL, Bauer W, Urbatsch IL. Bradford Assay for Determining Protein Concentration. Cold Spring Harb Protoc. 2020;2020(4):102269.

60.	Burnett SD, Blanchette AD, Chiu WA, Rusyn I. Human induced pluripotent stem cell (iPSC)-derived cardiomyocytes as an in vitro model in toxicology: strengths and weaknesses for hazard identification and risk characterization. Expert Opin Drug Metab Toxicol. 2021;17(8):887-902.

61.	Livak KJ, Schmittgen TD. Analysis of relative gene expression data using real-time quantitative PCR and the 2(-Delta Delta C(T)) Method. Methods. 2001;25(4):402-8.

62.	Wang S, Konorev EA, Kotamraju S, Joseph J, Kalivendi S, Kalyanaraman B. Doxorubicin induces apoptosis in normal and tumor cells via distinctly different mechanisms. intermediacy of H(2)O(2)- and p53-dependent pathways. J Biol Chem. 2004;279(24):25535-43.

63.	Liu J, Mao W, Ding B, Liang CS. ERKs/p53 signal transduction pathway is involved in doxorubicin-induced apoptosis in H9c2 cells and cardiomyocytes. Am J Physiol Heart Circ Physiol. 2008;295(5):H1956-65.

64.	Wang J, Zhao J, Shi M, Ding Y, Sun H, Yuan F, et al. Elevated Expression of miR-210 Predicts Poor Survival of Cancer Patients: A Systematic Review and Meta-Analysis. PLOS ONE. 2014;9(2):e89223.

65.	Emami Nejad A, Najafgholian S, Rostami A, Sistani A, Shojaeifar S, Esparvarinha M, et al. The role of hypoxia in the tumor microenvironment and development of cancer stem cell: a novel approach to developing treatment. Cancer Cell Int. 2021;21(1):62.

66.	Huang X, Ding L, Bennewith KL, Tong RT, Welford SM, Ang KK, et al. Hypoxia-inducible mir-210 regulates normoxic gene expression involved in tumor initiation. Mol Cell. 2009;35(6):856-67.

67.	Dang K, Myers KA. The Role of Hypoxia-Induced miR-210 in Cancer Progression. International Journal of Molecular Sciences. 2015;16(3):6353-72.

68.	Folkehelseinstituttet. Reseptregisteret [Internett]. 2021. [Hentet 10. oktober 2021]. Tilgjengelig fra: http://www.reseptregisteret.no/.

69.	Vaupel P, Multhoff G. Revisiting the Warburg effect: historical dogma versus current understanding. The Journal of Physiology. 2021;599(6):1745-57.

70.	Stamm P, Kirmes I, Palmer A, Molitor M, Kvandova M, Kalinovic S, et al. Doxorubicin induces wide-spread transcriptional changes in the myocardium of hearts distinguishing between mice with preserved and impaired cardiac function. Life Sciences. 2021;284:119879.

71.	Pereira JD, Tosatti JAG, Simões R, Luizon MR, Gomes KB, Alves MT. microRNAs associated to anthracycline-induced cardiotoxicity in women with breast cancer: A systematic review and pathway analysis. Biomed Pharmacother. 2020;131:110709.

72.	Rosenfeld R, Riondino S, Formica V, Torino F, Martuscelli E, Roselli M. MiRNAs and circRNAs for the Diagnosis of Anthracycline-Induced Cardiotoxicity in Breast Cancer Patients: A Narrative Review. J Pers Med. 2022;12(7).

73.	Zhu Z, Li X, Dong H, Ke S, Zheng WH. Let-7f and miRNA-126 correlate with reduced cardiotoxicity risk in triple-negative breast cancer patients who underwent neoadjuvant chemotherapy. Int J Clin Exp Pathol. 2018;11(10):4987-95.

74.	Cui C, Cui Q. The relationship of human tissue microRNAs with those from body fluids. Sci Rep. 2020;10(1):5644.

75.	Thermo Fisher Scientific. Useful numbers for cell culture [Internet]. 2024 [cited 2024 May 26]. Available from: https://tools.thermofisher.com/content/sfs/appendix/Cell_Culture/cell%20culture%20useful%20numbers.pdf.

76.	Thermo Fisher Scientific. Precision of qPCR [Internet]. 2024 [cited 2024 May 26]. Available from: https://www.thermofisher.com/no/en/home/life-science/pcr/real-time-pcr/real-time-pcr-learning-center/gene-expression-analysis-real-time-pcr-information/precision-qpcr.html.

77.	Tuomainen T, Tavi P. The role of cardiac energy metabolism in cardiac hypertrophy and failure. Exp Cell Res. 2017;360(1):12-8.

78.	Chan SY, Zhang YY, Hemann C, Mahoney CE, Zweier JL, Loscalzo J. MicroRNA-210 controls mitochondrial metabolism during hypoxia by repressing the iron-sulfur cluster assembly proteins ISCU1/2. Cell Metab. 2009;10(4):273-84.

79.	Rast G, Kraushaar U, Buckenmaier S, Ittrich C, Guth BD. Influence of field potential duration on spontaneous beating rate of human induced pluripotent stem cell-derived cardiomyocytes: Implications for data analysis and test system selection. J Pharmacol Toxicol Methods. 2016;82:74-82.

80.	Dean YE, Dahshan H, Motawea KR, Khalifa Z, Tanas Y, Rakha I, et al. Anthracyclines and the risk of arrhythmias: A systematic review and meta-analysis. Medicine (Baltimore). 2023;102(46):e35770.
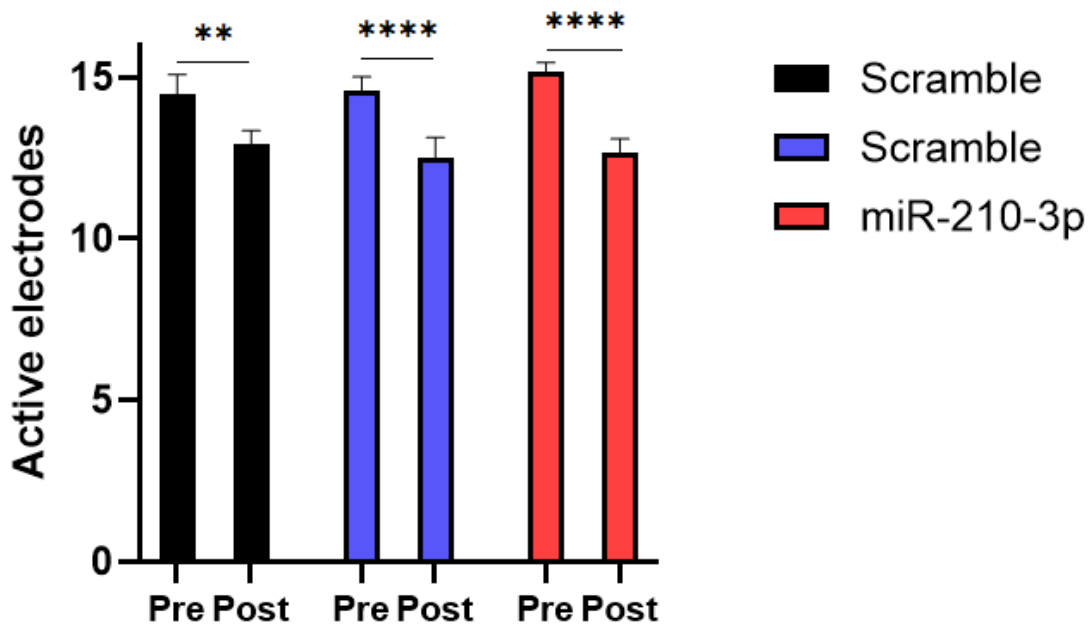
Appendices

Appendix I

Figure 11: Active electrodes before and after transfection. The data is presented as the mean ± SEM. SEM: Standard error of the mean. ** = p < 0.01, **** = p < 0.0001. miR-210: MicroRNA-210, DOX: Doxorubicin. Statistics were performed with a one-way ANOVA, with Tukey's multiple comparisons test. After treatment with scramble or miR-210-3p, the cells' activity was measured overnight using the MEA system. The transfection procedure significantly decreased the number of active electrodes in the control group (p < 0.01), scramble group (p < 0.0001) and miR-210 group (p < 0.0001), but no statistical difference was found between the different experimental groups before or after transfection.
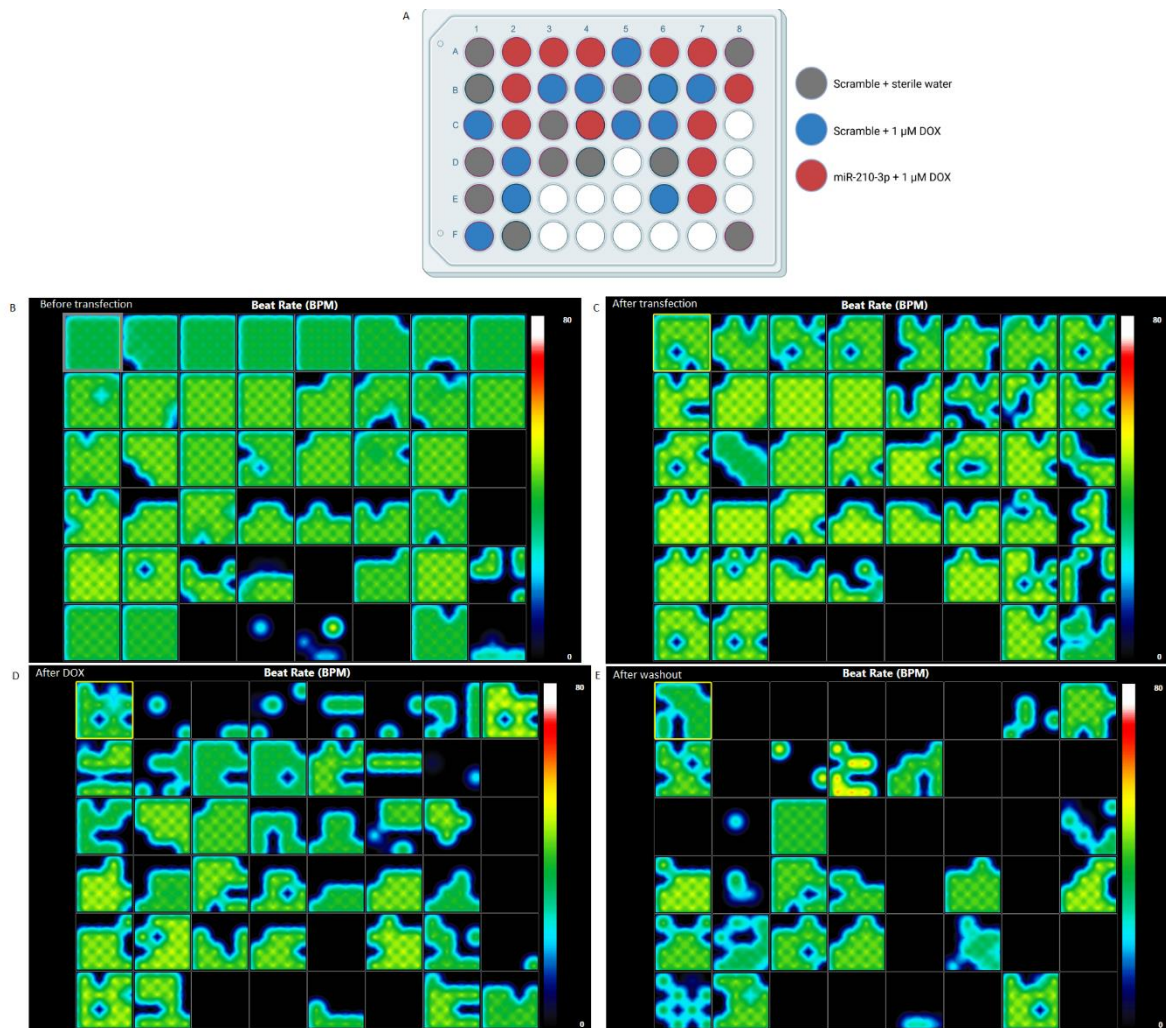
Appendix II

Figure 12: Experimental outline and heatmap of main experiment using hiPSC–CMs.
Experimental setup on MEA plate (A). Heatmap of MEA plate activity before transfection (B), after transfection (C), after DOX treatment (D) and after washout (E). DOX: Doxorubicin. MEA: Multiwell microelectrode array. H-iPSC-CM: Human induced pluripotent stem cell cardiomyocytes.